2018 Fall

"Phase Transformation *in* Materials"

11.29.2018

Eun Soo Park

Office: 33-313
Telephone: 880-7221
Email: espark@snu.ac.kr
Office hours: by an appointment

Contents for previous class

< Phase Transformation in Solids >

1) Diffusional Transformation (a) Precipitation

Q1: Overall Transformation Kinetics–TTT diagram

"Johnson-Mehl-Avrami Equation"

Q2: Precipitation in Age-Hardening Alloys

Q3: Age Hardening

Q4: How can you design an alloy with high strength at high T?

Q5: Quenched-in vacancies vs Precipitate-free zone

Contents for today's class

< Phase Transformation in Solids >

1) Diffusional Transformation (a) Precipitation

Q6: Spinodal Decomposition

Q7: Precipitation of Ferrite from Austenite (γ→α)

(b) Eutectoid Transformation (5.8 절)

(c) Order-disorder Transformation (1.3.7 절)

(d) Massive Transformation (5.9 절)

(e) Polymorphic Transformation

Q6: Spinodal Decomposition

5.5.5 Spinodal Decomposition

Spinodal mode of transformation has no barrier to nucleation

: describing the transformation of a system of two or more components in a metastable phase into two stable phases

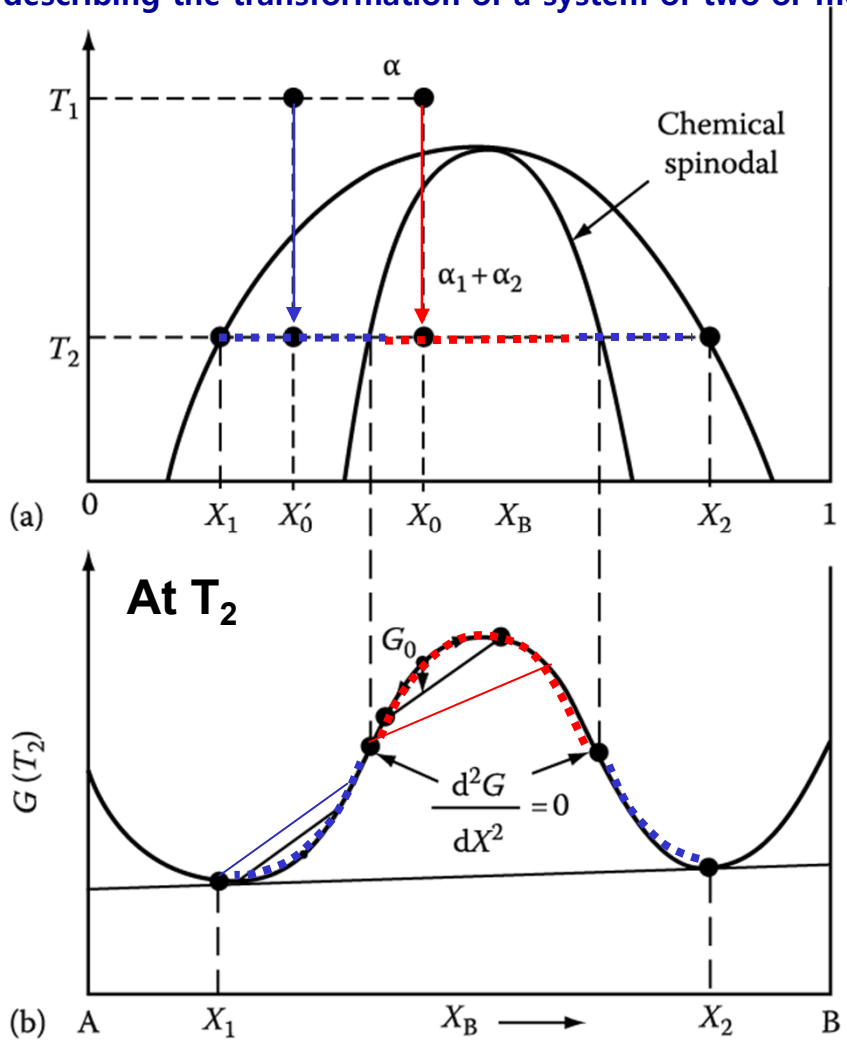

Fig. 5.38 Alloys between the spinodal points are unstable and can decompose into two coherent phasees α_1 and α_2 without overcoming an activation energy barrier. Alloys between the coherent miscibility gaps and the spinodal are metastable and can decompose only after nucleation of the other phase.

How does it differ between inside and outside the inflection point of Gibbs free energy curve?

1) Within the spinodal $\frac{d^2G}{dX^2}<0$

: phase separation by small fluctuations in composition/ "up-hill diffusion"

2) If the alloy lies outside the spinodal, small variation in composition leads to an increase in free energy and the alloy is therefore metastable.

The free energy can only be decreased if nuclei are formed with a composition very different from the matrix.

→ **nucleation and growth**
: "down-hill diffusion"

a) Composition fluctuations within the spinodal

b) Normal down-hill diffusion outside the spinodal

up-hill diffusion

down-hill diffusion

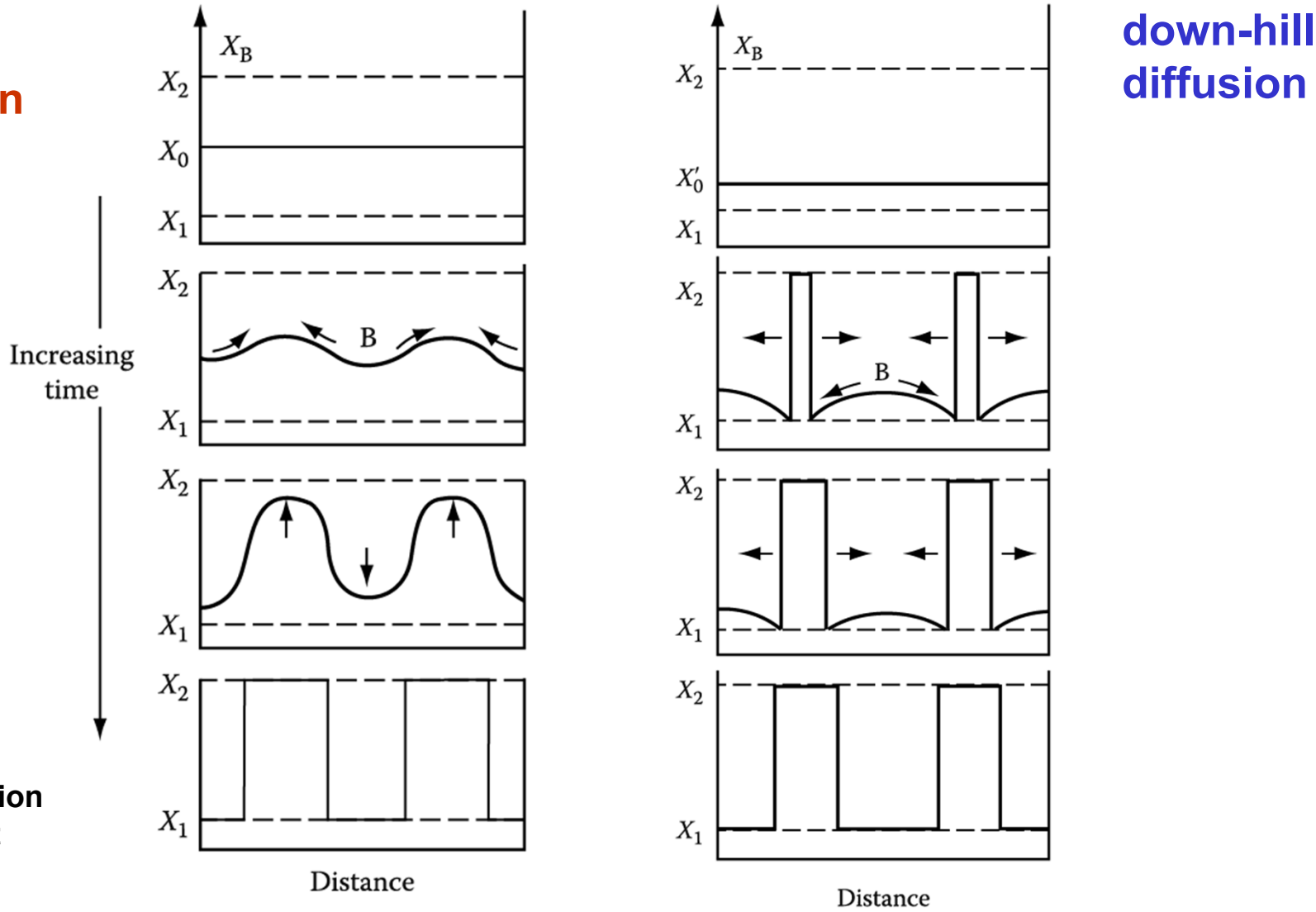

interdiffusion coefficient D<0

Fig. 5.39 & 5.40 schematic composition profiles at increasing times in (a) an alloy quenched into the spinodal region (X_0 in Figure 5.38) and (b) an alloy outside the spinodal points (X_0' in Figure 5.38)

Phase separation

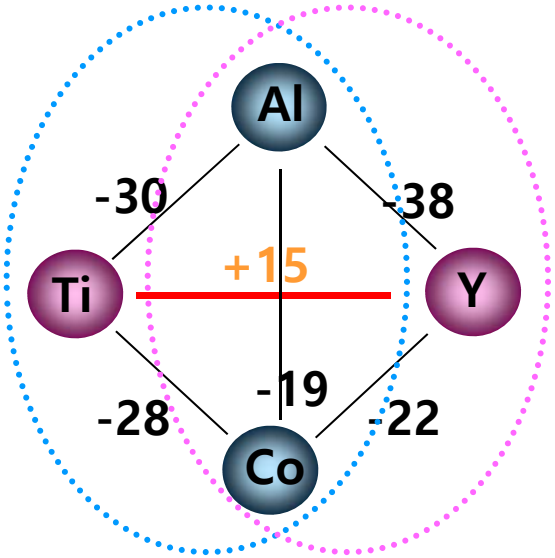

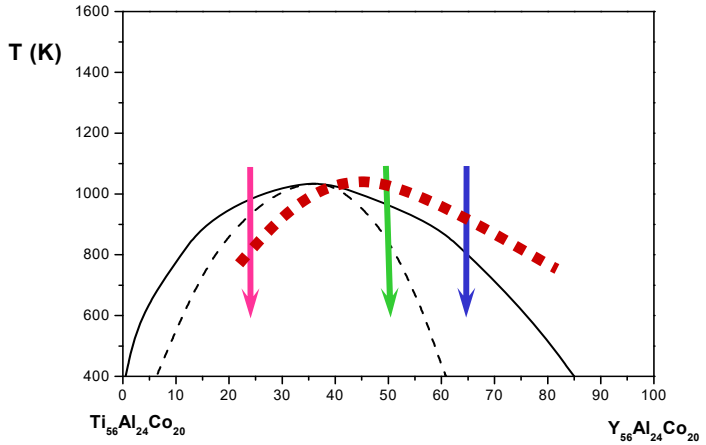

Droplet structure

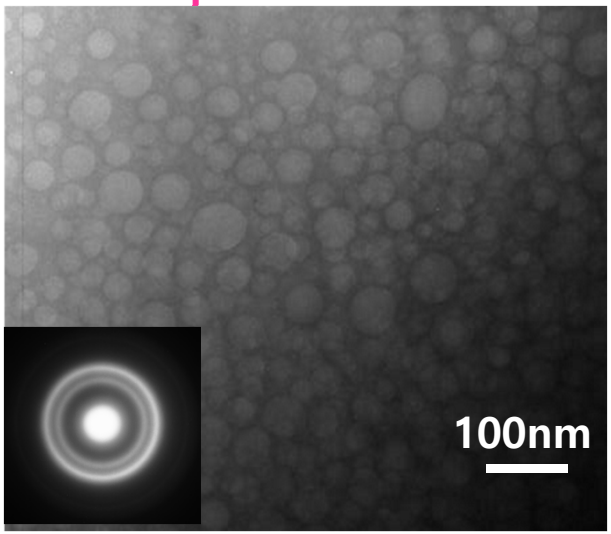

$(Y_{56}Al_{24}Co_{20})_{25}(Ti_{56}Al_{24}Co_{20})_{75}$

Interconnected structure

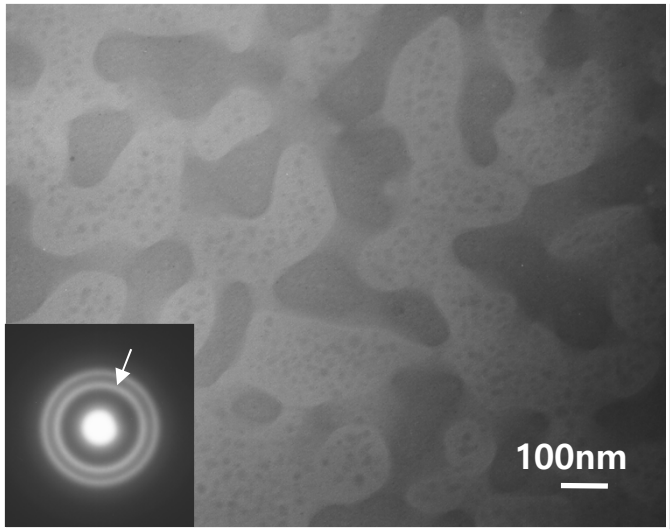

$(Y_{56}Al_{24}Co_{20})_{50}(Ti_{56}Al_{24}Co_{20})_{50}$

Droplet structure

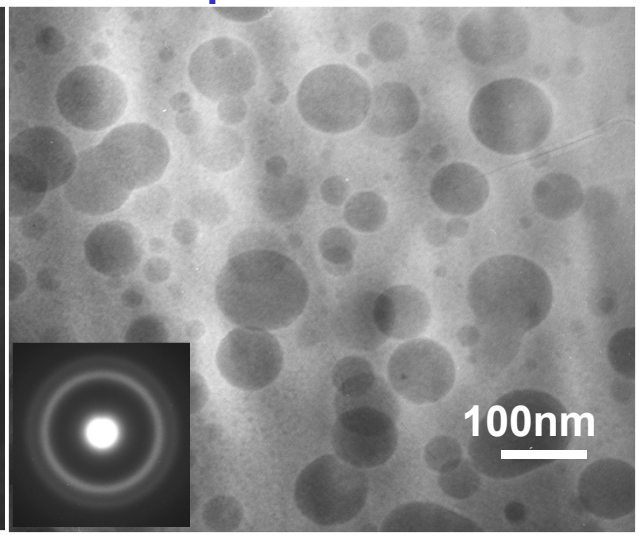

$(Y_{56}Al_{24}Co_{20})_{65}(Ti_{56}Al_{24}Co_{20})_{35}$

5.5.5 Spinodal Decomposition

* The Rate of Spinodal decomposition

a) Rate controlled by interdiffusion coefficient D (상호확산계수)

Within the spinodal D < 0,

composition fluctuation $\propto \exp(-t/\tau)$

(next page)

$$\tau = -\lambda^2 / 4\pi^2 D$$

τ: characteristic time constant

λ: wavelength of the composition modulations

(assumed one-dimensional)

b) Kinetics depends on λ: Transformation rate ↑ as λ ↓ (as small as possible).

But, minimum value of λ below which spinodal decomposition cannot occur.

Solutions to the diffusion equations

Ex1. Homogenization of sinusoidal varying composition in the elimination of segregation in casting

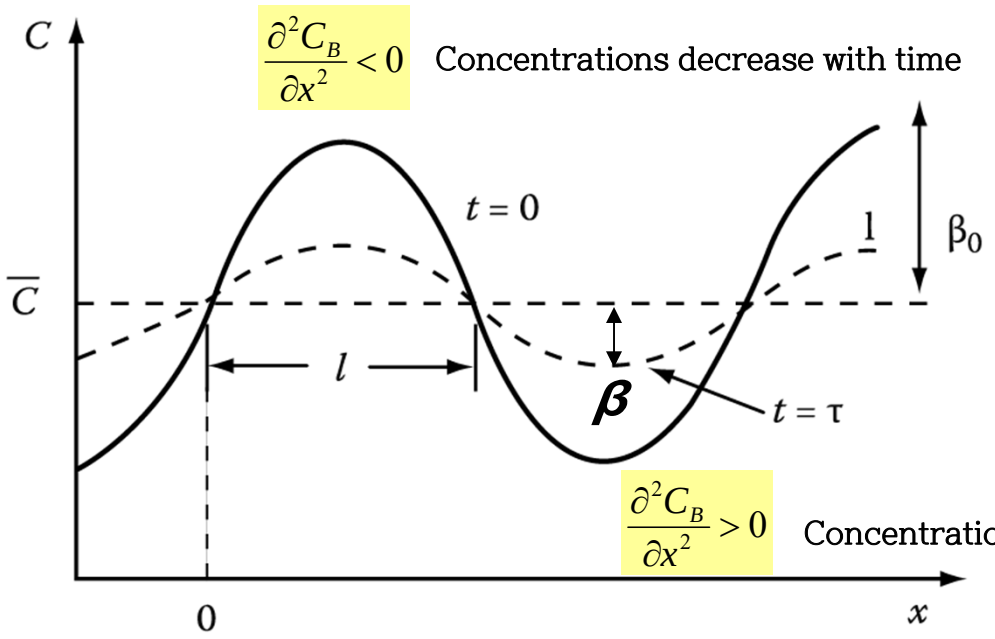

Fig. 2.10 The effect of diffusion on a sinusoidal variation of composition.

$$C = \overline{C} + \beta_0 \sin\frac{\pi x}{l} \quad \text{at t=0}$$

$$C = \overline{C} + \beta_0 \sin\frac{\pi x}{l}\exp\left(\frac{-t}{\tau}\right)$$

$$\beta = \beta_0 \exp(-t/\tau) \quad at \quad x = \frac{l}{2}$$

Amplitude of the concentration profile (β) decreases exponentially with time, $C \Rightarrow \overline{C}$

$$\tau = \frac{l^2}{\pi^2 D}$$

τ : relaxation time

"decide homogenization rate"

The initial concentration profile will not usually be sinusoidal, but in general any concentration profile can be considered as the sum of an infinite series of sine waves of varying wavelength and amplitude, and each wave decays at a rate determined by its own "τ". Thus, the short wavelength terms die away very rapidly and the homogenization will ultimately be determined by τ for the longest wavelength component.

* **Calculation of the wavelength (λ) of the composition fluctuations**

→ **Free Energy change for the decomposition**

1) Decomposition of X_0 into $X_0 + \Delta X$ and $X_0 - \Delta X$

What would be an additional energy affecting spinodal decomposition?

In practice, it is necessary to consider two important factors

2) interfacial energy

3) coherency strain energy

1) Decomposition of X_0 into $X_0 + \Delta X$ and $X_0 - \Delta X$

$$\Delta G_{chem} = \frac{1}{2}\frac{d^2G}{dX^2}(\Delta X)^2$$

Gibb's free energy reduction by compositional change

$$f(a+h) = f(a) + f'(a)h + \frac{f''(a)}{2!}h^2 + \cdots$$

$$G(X_0 + \Delta X) \approx G(X_0) + G'(X_0)\Delta X + \frac{G''(X_0)}{2!}\Delta X^2$$

$$G(X_0 - \Delta X) \approx G(X_0) - G'(X_0)\Delta X + \frac{G''(X_0)}{2!}\Delta X^2$$

$$\Delta G_{chem} = \frac{G(X_0 + \Delta X) + G(X_0 - \Delta X)}{2} - G(X_0)$$

$$= \frac{G''(X_0)}{2!}\Delta X^2 = \frac{1}{2}\frac{d^2G}{dX^2}\Delta X^2$$

5.5.5 Spinodal Decomposition

2) During the early stages, the interface between A-rich and B-rich region is not sharp but very diffuse. → diffuse interface

ΔG by formation of interface btw decomposed phases

Interfacial Energy
(gradient energy)

∝ composition gradient across the interface
: increased # of unlike nearest neighbors in a solution containing composition gradients

$$\Delta G_\gamma = K\left(\frac{\Delta X}{\lambda}\right)^2$$

Max. compositional gradient ΔX/λ

K : a proportionality constant dependent on the difference in the bond energies of like and unlike atom pair

If the size of the atoms making up the solid solution are different, the generation of composition differences, ΔX will introduce a coherency strain energy term, ΔGs.

3) Coherency Strain Energy
(atomic size difference)

$$\Delta G_S \propto E\delta^2 \Leftarrow \delta = (da/dX)\,\Delta X/a$$

δ: misfit between the A-rich & B-rich regions, E: Young's modulus, a: lattice parameter

$$\Delta G_S = \eta^2(\Delta X)^2 E' V_m$$

$$\text{where } \eta = \frac{1}{a}\left(\frac{da}{dX}\right), E' = E/(1-\nu)$$

ΔGs~ independent of λ

η: the fractional change in lattice parameter per unit composition change

*** Total free E change by the formation of a composition fluctuation 1) + 2) + 3)**

$$\Delta G = \left\{\frac{d^2G}{dX^2} + \frac{2K}{\lambda^2} + 2\eta^2 E' V_m\right\}\frac{(\Delta X)^2}{2}$$

5.5.5 Spinodal Decomposition

* Total free E change by the formation of a composition fluctuation

$$\Delta G = \left\{ \frac{d^2G}{dX^2} + \frac{2K}{\lambda^2} + 2\eta^2 E' V_m \right\} \frac{(\Delta X)^2}{2} < 0$$

a) Condition for Spinodal Decomposition

(→ a homogeneous solid solution~unstable)

$$-\frac{d^2G}{dX^2} > \frac{2K}{\lambda^2} + 2\eta^2 E' V_m$$

b) The Limit of T and composition in coherent spinodal decomposition

(스피노달 분해가 일어나는 온도와 조성의 한계값)

$$\lambda \to \infty$$

$$\frac{d^2G}{dX^2} = -2\eta^2 E' V_m$$

→ **coherent spinodal**

It lies entirely within the chemical spinodal ($d^2G/dX^2=0$)

(boundary btw ③ & ④, next page)

Wavelength for coherent spinodal

$$\lambda^2 > -2K \Big/ \left(\frac{d^2G}{dX^2} + 2\eta^2 E' V_m \right)$$

→ The minimum possible wavelength (λ) decreases with increasing undercooling (ΔT~ΔX) below the coherent spinodal.

This figure include the lines defining the equilibrium compositions of the coherent/ incoherent phases that result from spinodal decomposition.

* Incoherent(or equilibrium) miscibility gap: $\Delta H > 0$

The miscibility gap the normally appears on an equilibrium phase is the incoherent (or equilibrium) miscibility gap.→ equilibrium compositions of incoherent phases without strain fields.

a) **chemical spinodal: $d^2G/dX^2=0$_no practical importance X**

b) **Area ② , ΔG_V-ΔG_S < 0 → only incoherent strain-free nuclei can form.**

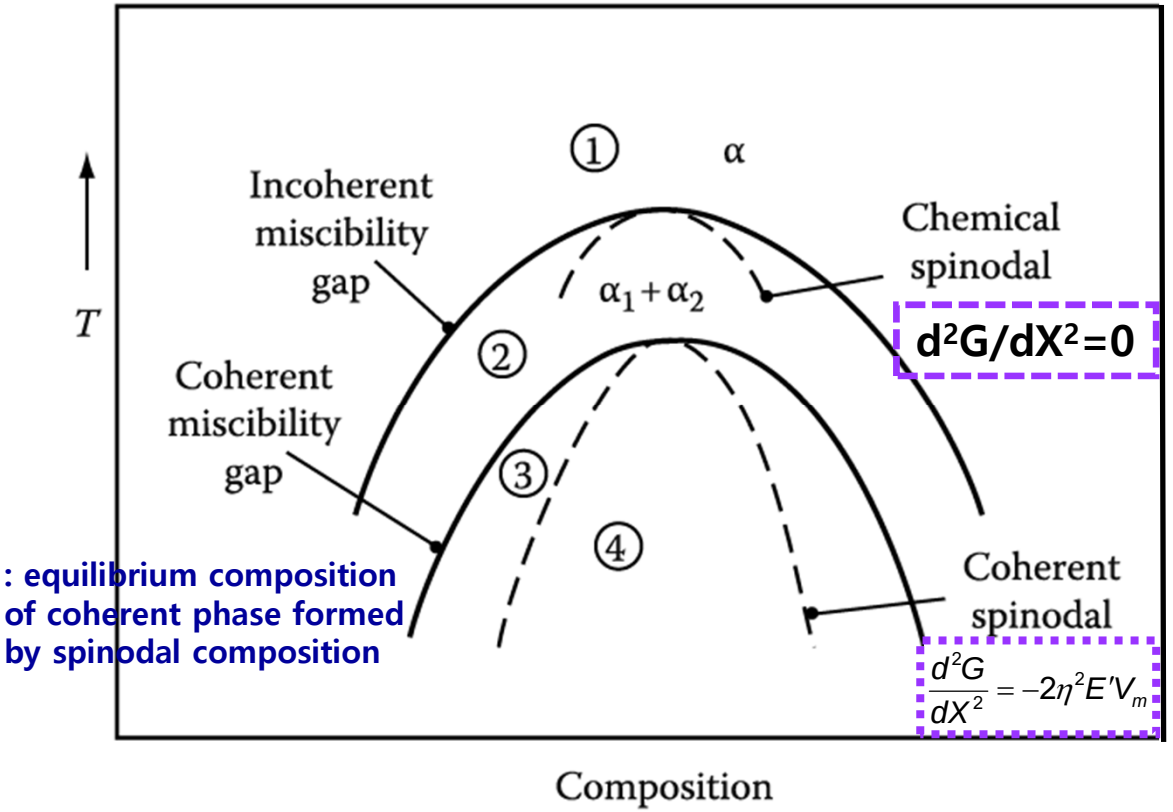

Figure 5.41 Schematic phase diagram for a clustering system.

Region 1: homogeneous α stable. Region 2: homogeneous α metastable, only incoherent phases can nucleate. Region 3: homogeneous α metastable, coherent phase can nucleate. Region 4: homogeneous α unstable, no nucleation barrier, spinodal decomposition occurs.

Spinodal decomposition is not only limited to systems containing a stable miscibility gap

All systems in which *GP zones* form, for example, containing a metastable coherent miscibility gap, i.e., the GP zone solvus.

→ at high supersaturation, GP zone can form by the spinodal mechanism.

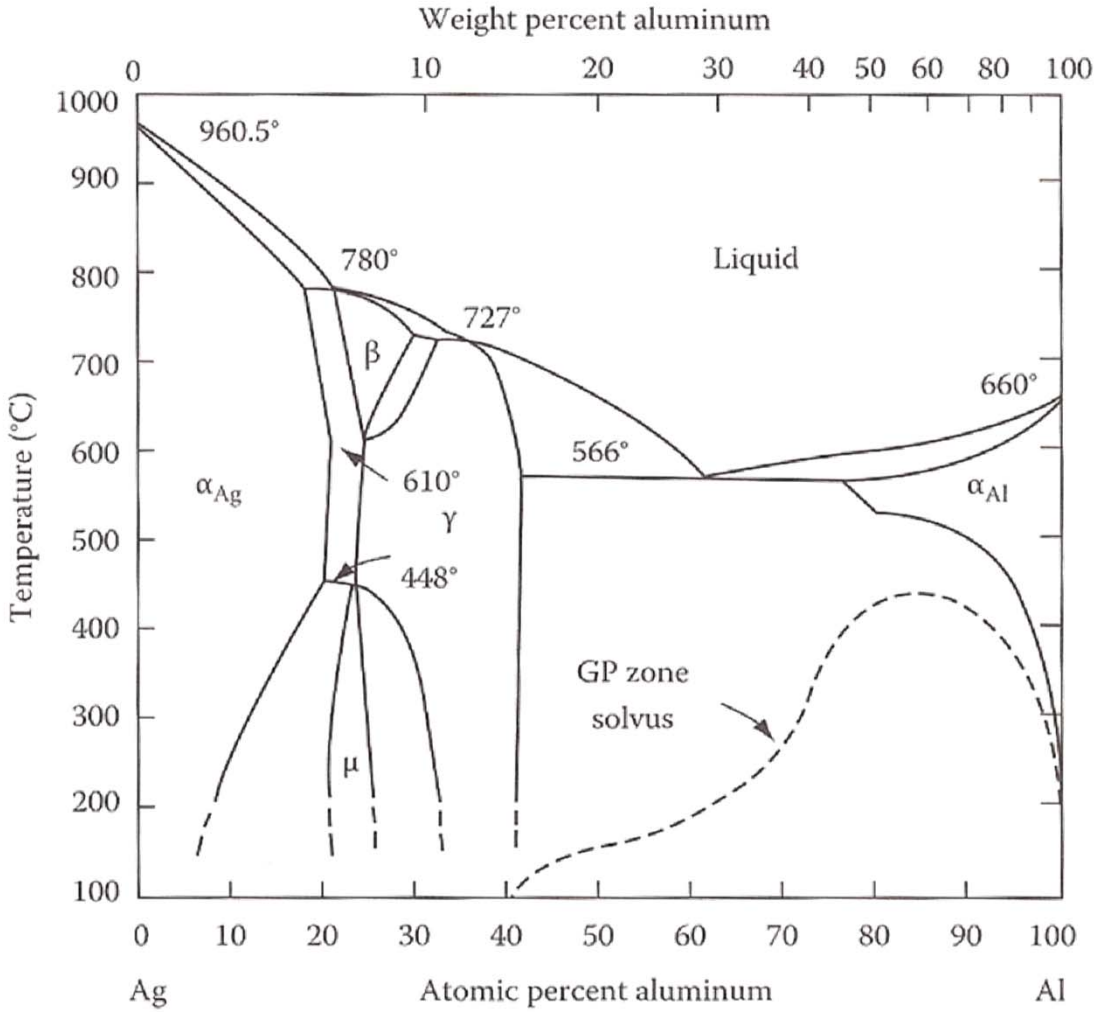

Figure 5.34

Al-Ag phase diagram showing metastable two-phase field corresponding to GP zones.

- The difference in T between the coherent and incoherent miscibility gaps, or the chemical and coherent spinodals $\propto$ **magnitude of** $|\eta|$ η: the fractional change in lattice parameter per unit composition change
- Large atomic size difference → $|\eta|$ **large**→large undercooling to overcome the strain E effects
- Like Al-Cu, large values of $|\eta|$ in cubic metals can be mitigated if the misfit strains are accommodated in the elastically soft <100> directions. → composition modulations building up normal to {100}

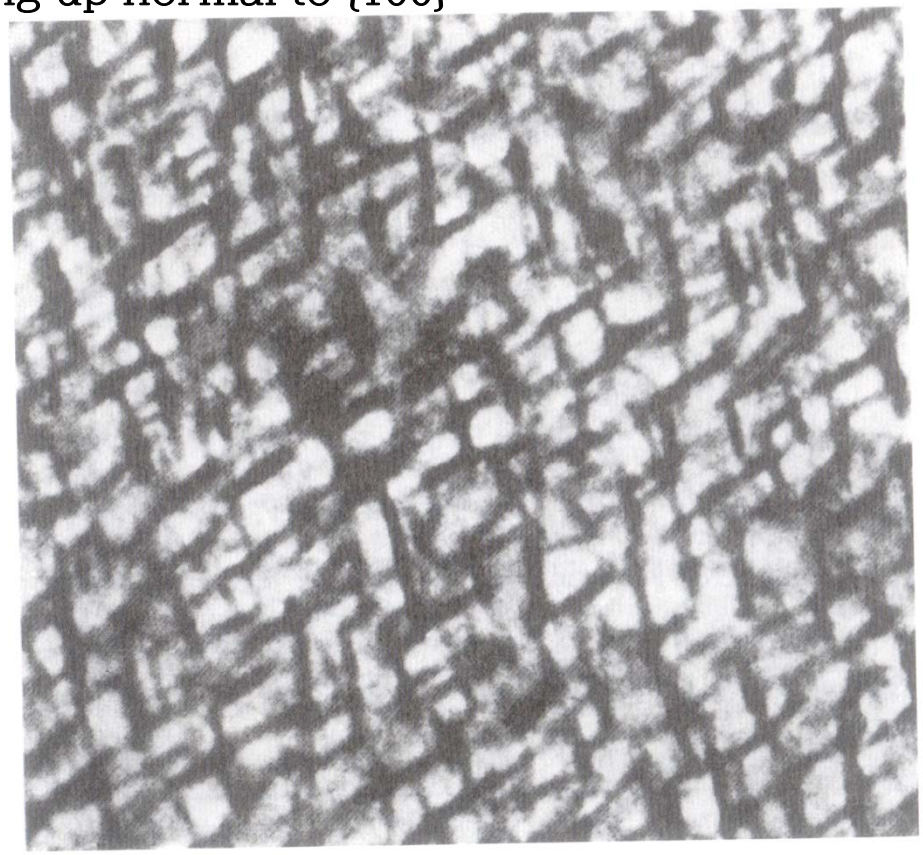

Figure 5.42 A coarsened spinodal microstructure in Al-22.5 Zn-0.1 Mg (at%) solution treated 2h at 400 ℃ and aged 20h at 100℃. Thin foil electron micrograph. λ = 25 nm_coarsening

Q7: Precipitation of Ferrite from Austenite ($\gamma \rightarrow \alpha$)

5.6. The Precipitation of Ferrite from Austenite (γ→α)

(Most important nucleation site: Grain boundary and the surface of inclusions)

The Iron-Carbon Phase Diagram

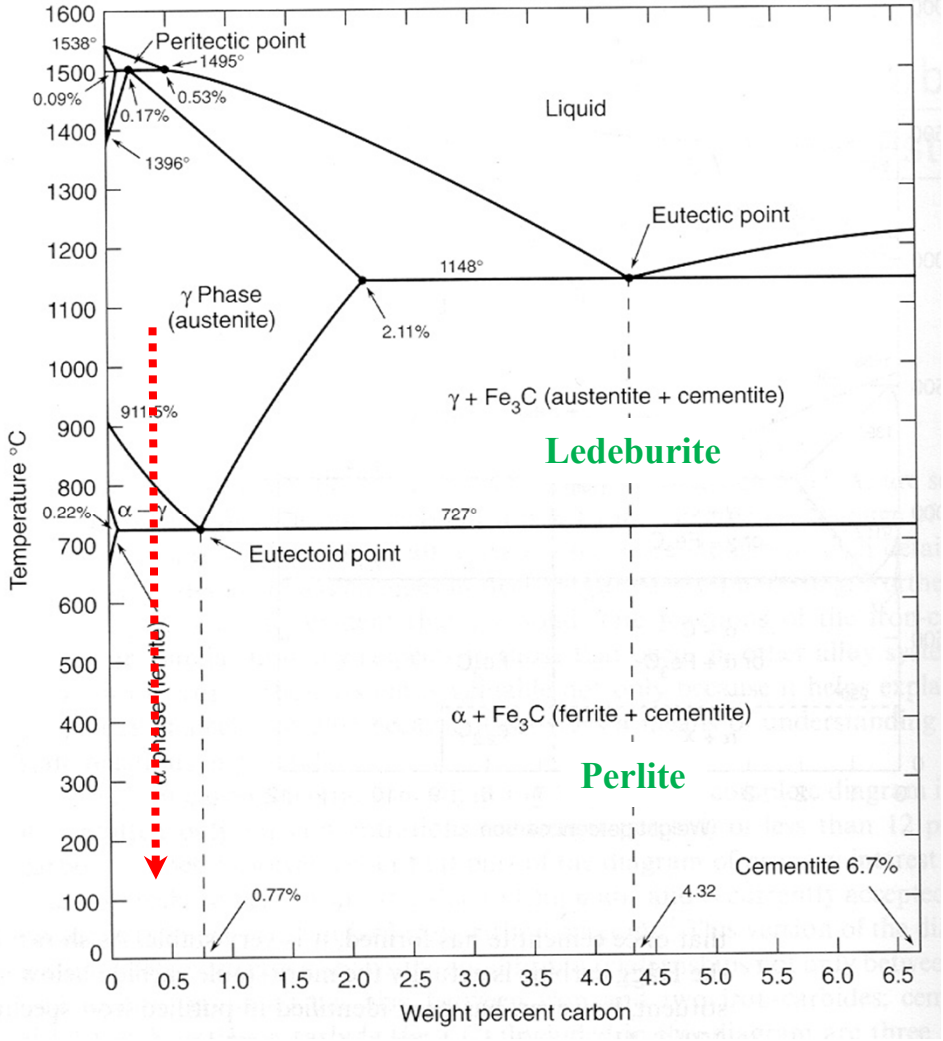

Microstructure (0.4 wt%C) evolved by slow cooling (air, furnace) ?

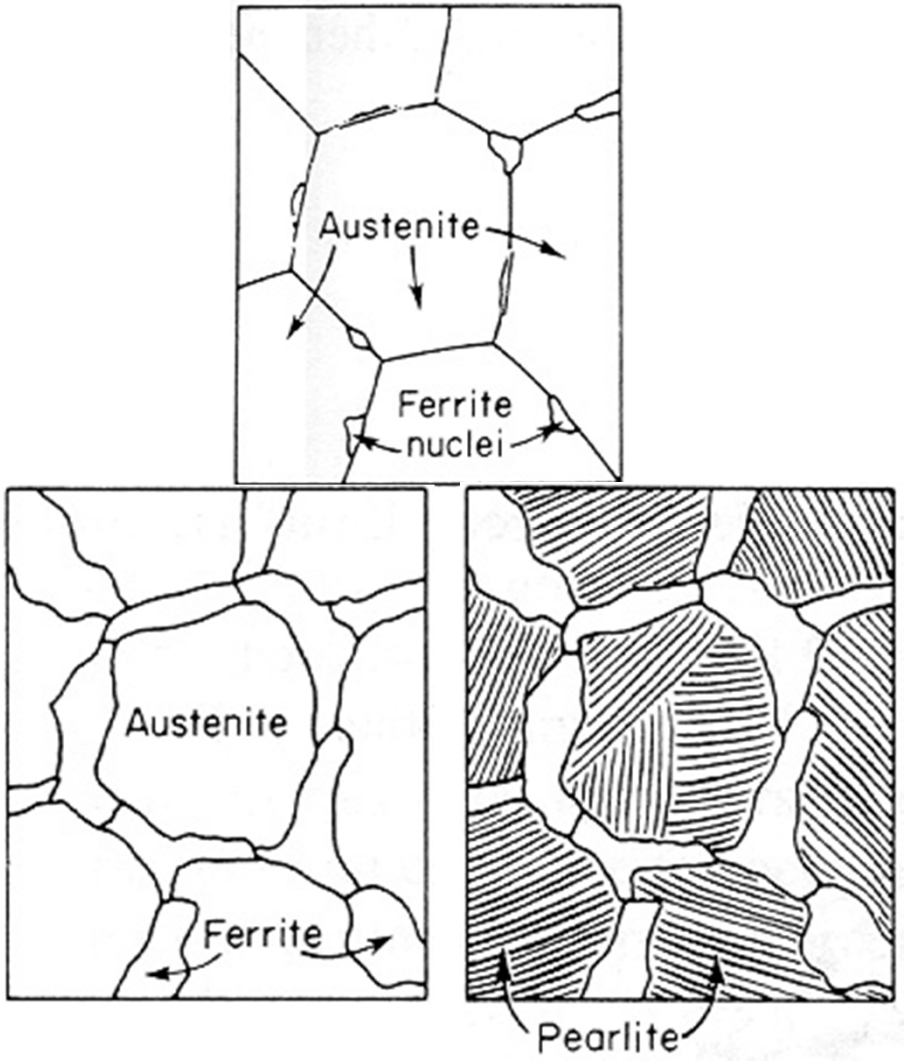

5.6. The Precipitation of Ferrite from Austenite

Diffusional Transformation of Austenite into Ferrite

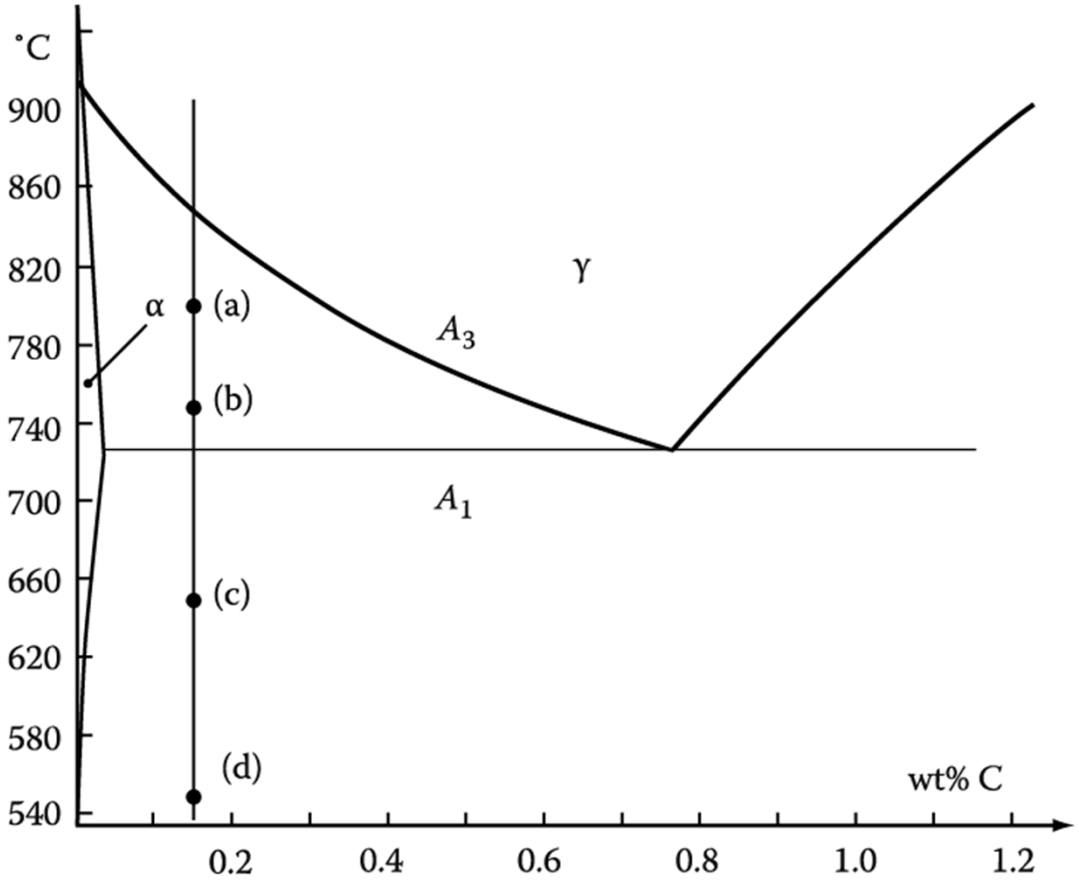

Figure 5.45 Holding temperature for steel in Figure. 5.46

Fe-0.15 wt%C

After being austenitized, held at

(a) 800°C for 150 s

(b) 750°C for 40 s

(c) 650°C for 9 s

(d) 550°C for 2 s and

then quenched to room T.

What would be the microstructures?

Microstructures of an austenitized Fe-0.15%C alloy (x 100 except (d, x300))

White: α ferrite/ Gray: M formed from untransformed γ/ fine constituent: a mixture of ferrite and carbide

Primary ferrite allotriomorphs with a few plates ⇨ Many more plates, mostly growing from GBs/ inside α grain

Smaller ΔT

(a)
800°C
for 150 s

(입계타형) G.B. allotriomorphs
"blockey" manner/
Smoothly curved & faceted α/γ
Interface are present

(b)
750°C
for 40 s

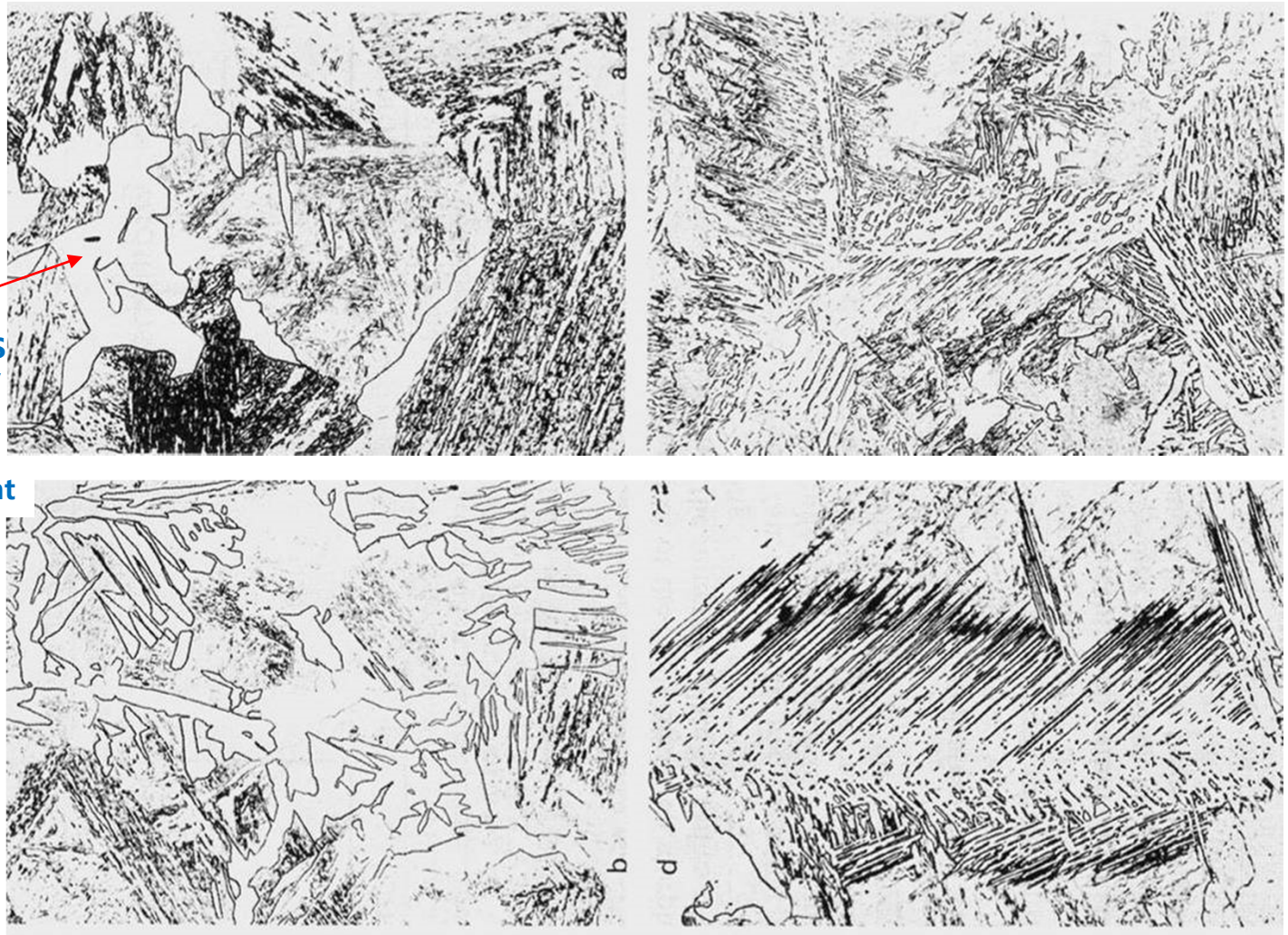

(c)
650°C
for 9 s

(d)
550°C
for 2 s

larger ΔT

Widmanstätten ferrite side-plates (b), (c), (d) _ Finer & faceted coherent interface with increasing "undercooling"

* Grain boundary allotriomorph 입계타형

Grain boundary precipitation → **Faster than allowed by volume diffusion**
involves three steps

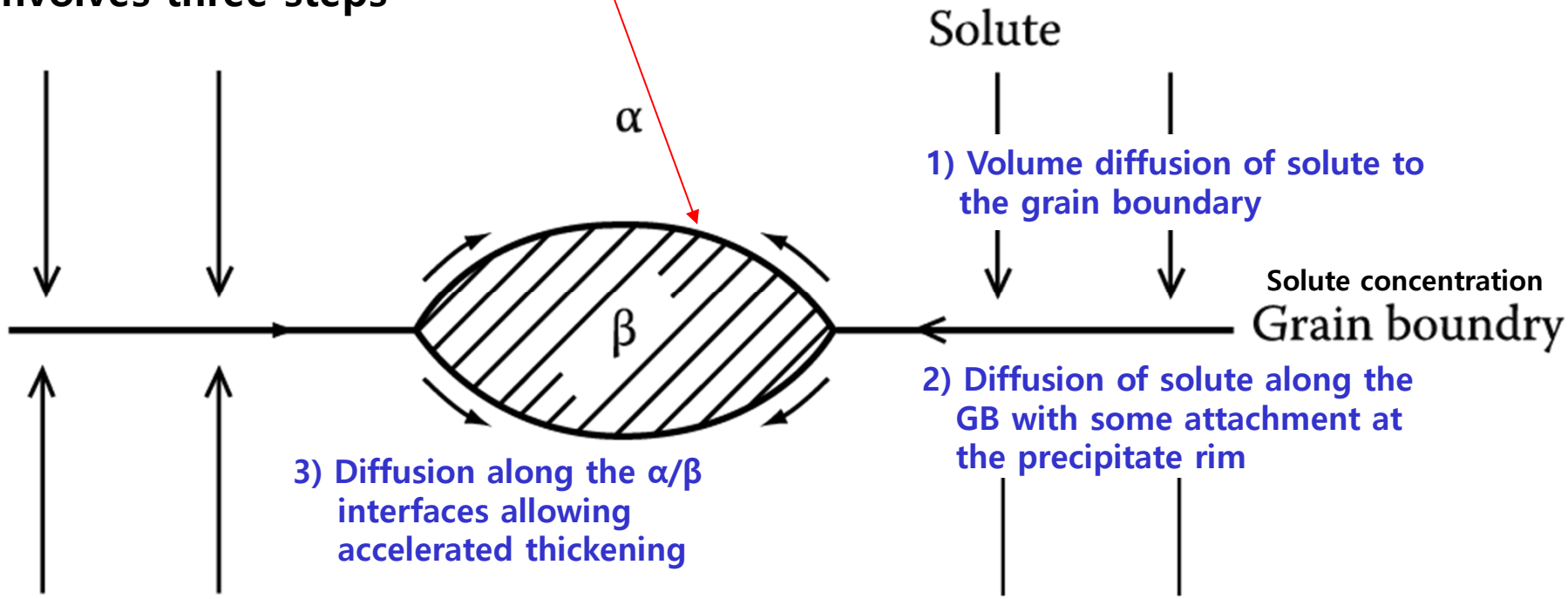

치환형 확산이 일어나는 경우 매우 중요/ 침입형 고용체에서는 체적 확산 속도가 크기 때문에 입계나 전위를 통한 단거리 확산은 상대적으로 중요하지 않음.

Fig. 5.18 Grain-boundary diffusion can lead to rapid lengthening and thickening of grain boundary precipitates, especially by substitutional diffusion.

The reason for the transition from grain boundary allotriomorphs to Widman -stätten side-plates with increasing undercooling is not fully understood.

→ possible answer: **Relative Velocity of Incoherent & Semicoherent Interfaces vary with undercooling**

a) At small undercoolings, both semi-coherent and incoherent interfaces ~similar rates

b) At large undercoolings, only incoherent interfaces~full use of increased driving force

(Continuous growth)

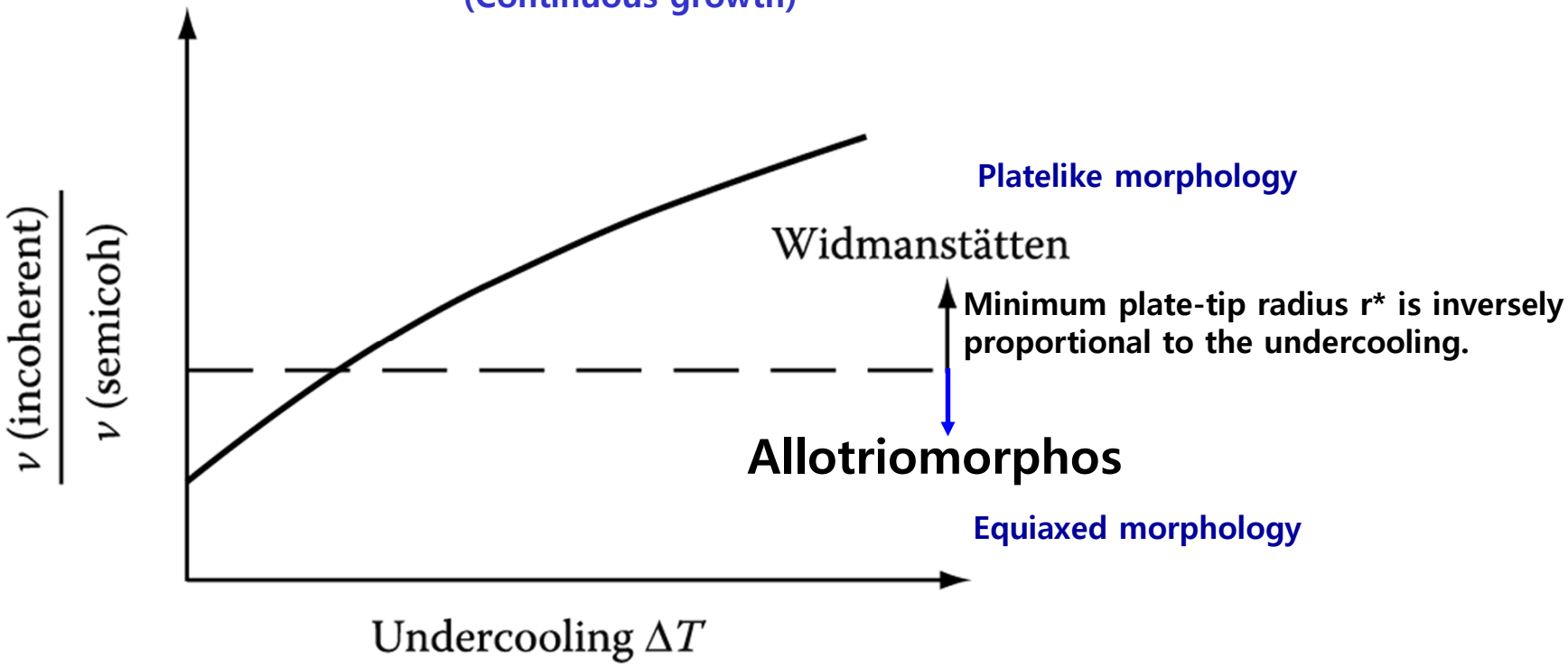

* Intragranular ferrite in large-grained specimen

: ferrite can also precipitate within the austenite grains (Fig. in page 17)
suitable heterogeneous nucleation site~inclusions and dislocations
generally equiaxed at low undercooling ↔ more platelike at higher undercolings

5.6. The Precipitation of Ferrite from Austenite

Typical TTT curve for $\gamma \rightarrow \alpha$ transformation $\rightarrow f(t,T)$

J-M-A Eq. $f = 1 - \exp(-kt^n)$

k: sensitive with T $f(I, v)$ $-\frac{\pi}{3} Iv^3$

n: 1 ~ 4 (depend on nucleation mechanism)

a) Time for a given percentage transformation will decrease as the constant k increase

b) k increases with increases in ΔT or total # of nucleation sites

→ Thus, decreasing the austenite grain size has the effect of shifting the C curve to shorter transformation times.

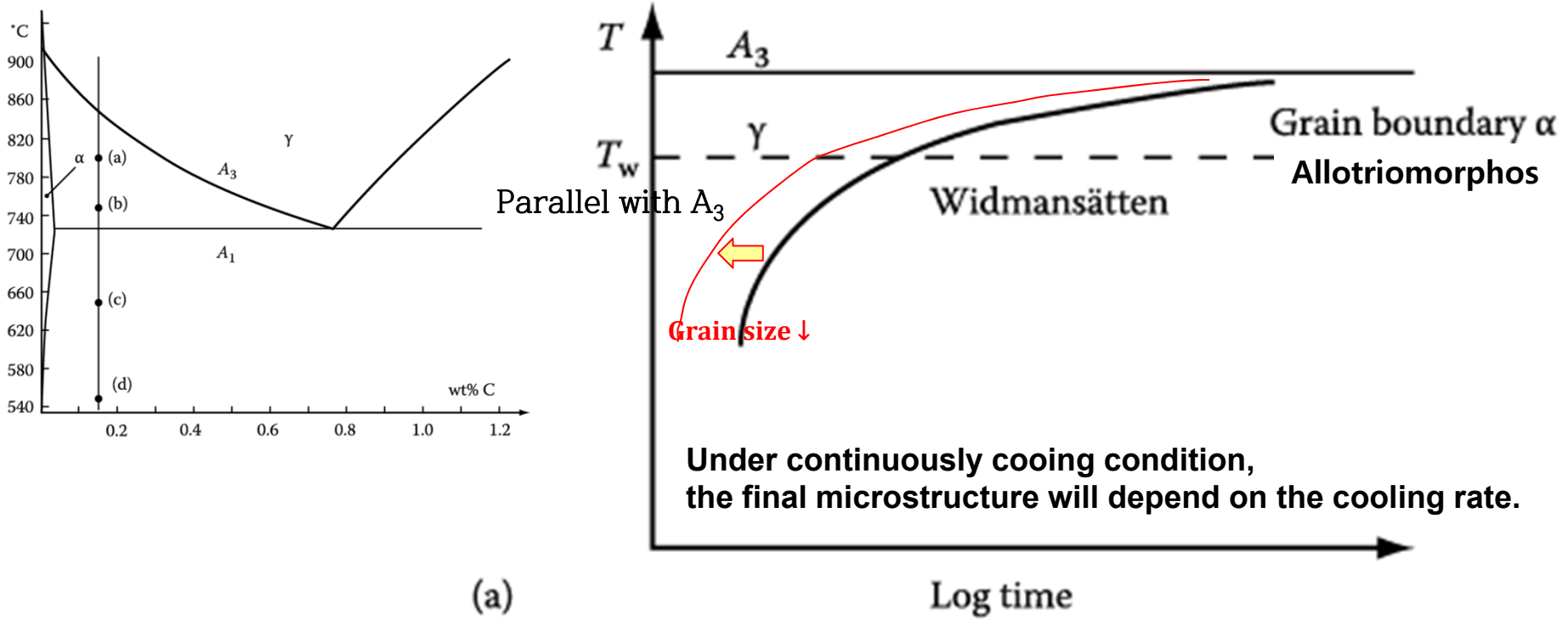

Figure 5.48 (a) typical TTT curve for $\gamma \rightarrow \alpha$ transformation in a hypoeutectoid steel: a typical C shape.

For alloys of different carbon content, A_3 and T_w vary and show parallel manner each other.

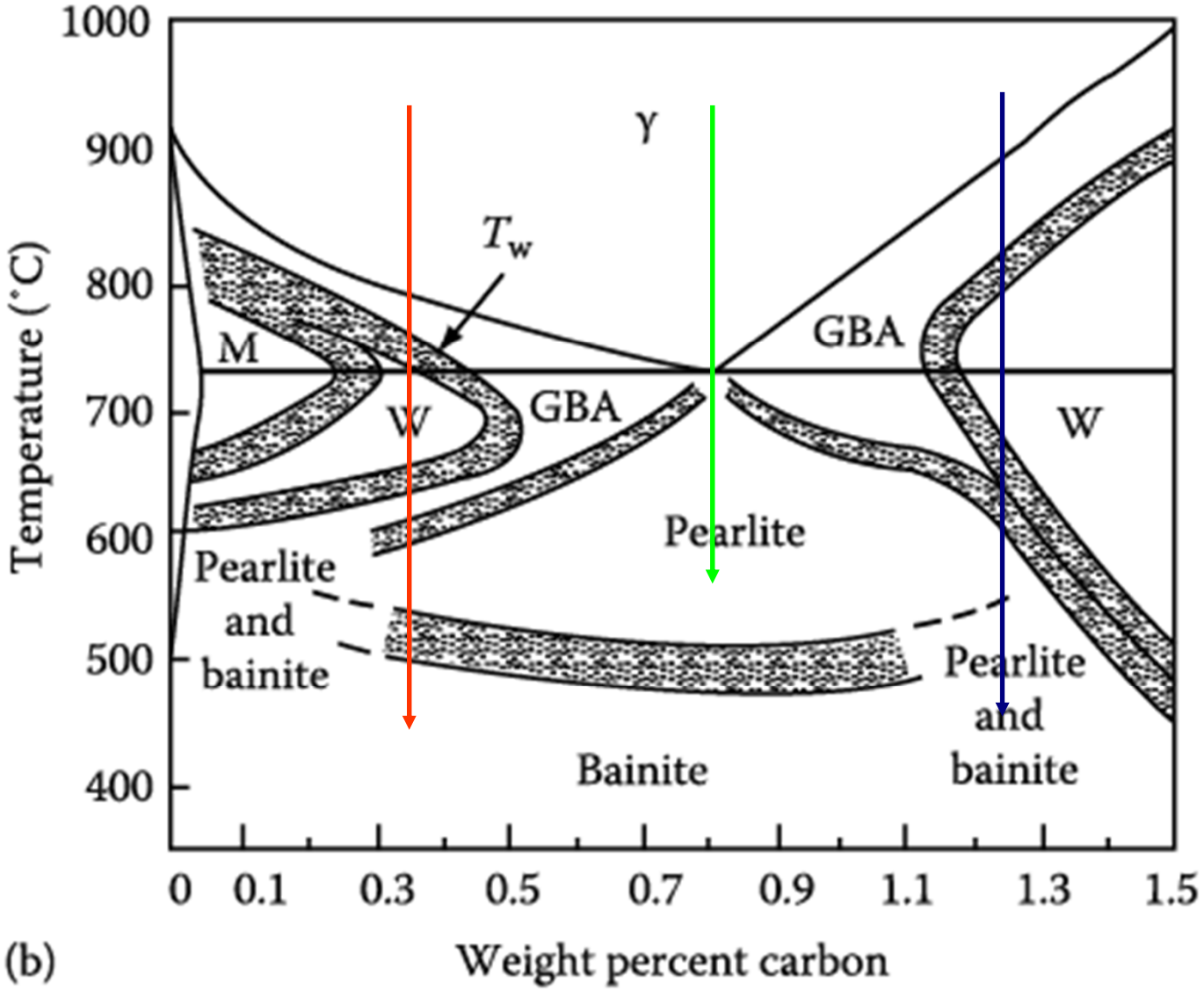

(GBA: GB allotriomorphs, W: Widmanstatten sideplates/intermolecular plates, M: Massive ferrite)

Figure 5.48 (b) Temperature-composition regions in which the various morphologies are dominant at late reaction times in specimens with ASTM grain size Nos. 0-1.

5.6.1 & 5.7 skip

5. Diffusion Transformations in solid

: diffusional nucleation & growth

(a) Precipitation

$$\alpha' \rightarrow \alpha + \beta$$

Metastable supersaturated
Solid solution

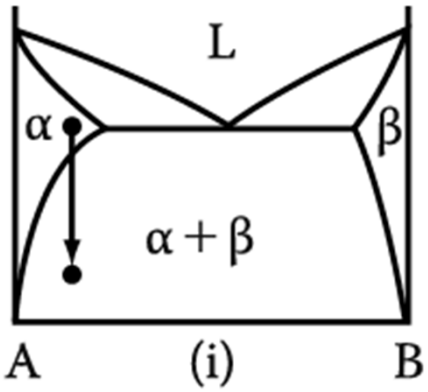

Homogeneous Nucleation

$$\Delta G = -V\Delta G_V + A\gamma + V\Delta G_S$$

$$N_{hom} = \omega C_0 \exp\left(-\frac{\Delta G_m}{kT}\right)\exp\left(-\frac{\Delta G^*}{kT}\right)$$

Heterogeneous Nucleation

$$\Delta G_{het} = -V(\Delta G_V - \Delta G_S) + A\gamma - \Delta G_d$$

➡ suitable nucleation sites ~ nonequilibrium defects
(creation of nucleus~destruction of a defect($-\Delta G_d$))

(b) Eutectoid Transformation

Composition of product phases differs from that of a parent phase.

→ **long-range diffusion**

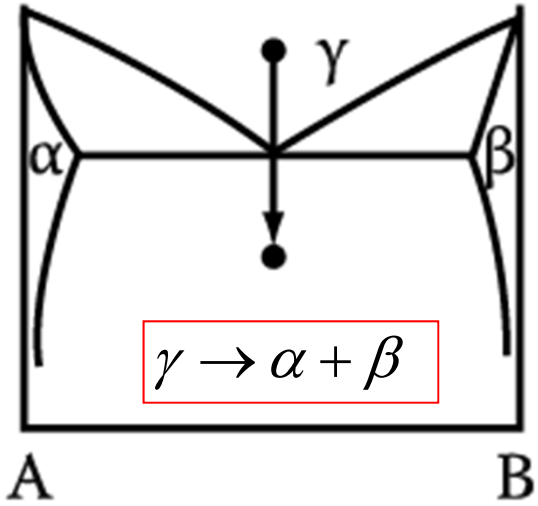

5.8. Eutectoid Transformation

5.8.1 Pearlite Reaction in Fe-C Alloys

$$\gamma \rightarrow \alpha + Fe_3C$$

Very similar to a eutectic transformation

Pearlite nodule nucleate on GBs and grow with a roughly constant radial velocity into the surrounding austenite grains.

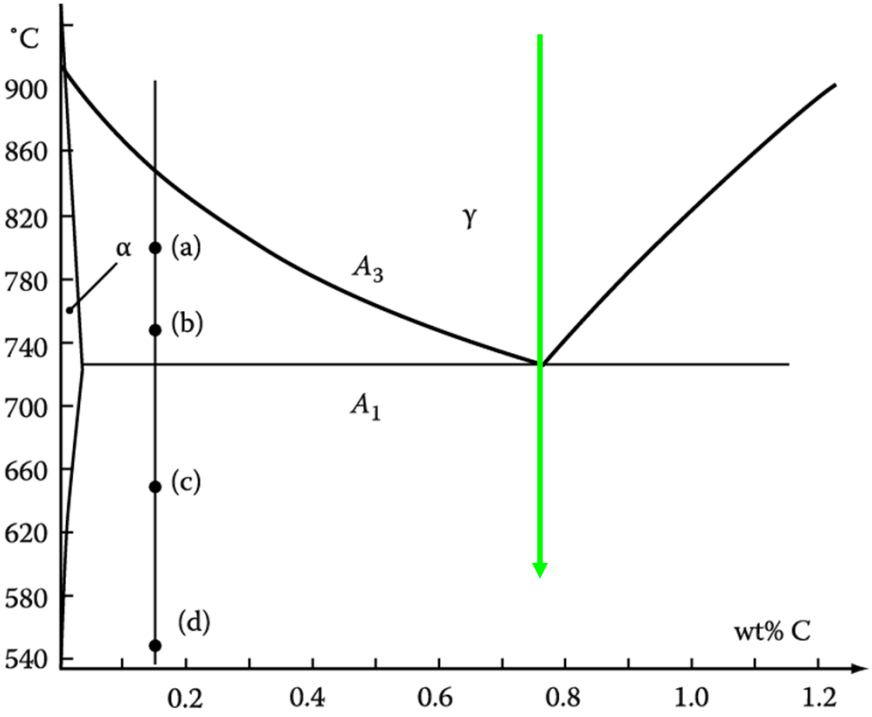

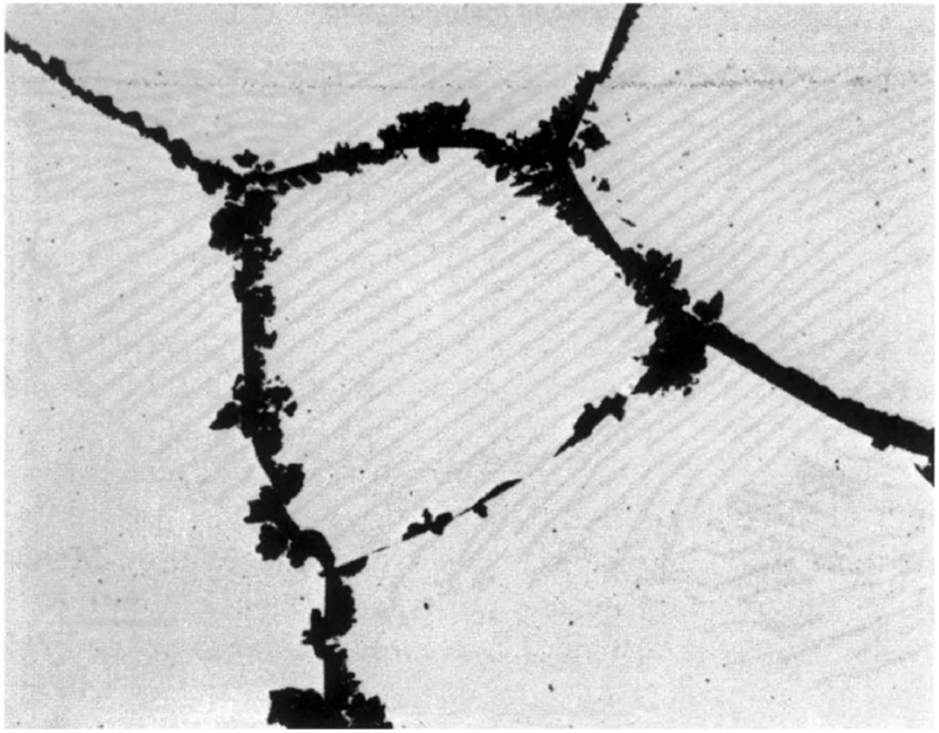

*** At large undercooling,**

: the nucleation rate is much higher and site saturation occurs, that is all GBs become quickly covered with nodules which grow together forming layers of perlite, Figure 5.61.

*** At small undercooling below A_1,**

: the number of pearlite nodules that nucleate is relatively small, and the nodules can grow as hemispheres or spheres without interfering with each other.

Pearlite Reaction in Fe-C Alloys: nucleation and growth

Nucleation: depend on GB structures and composition

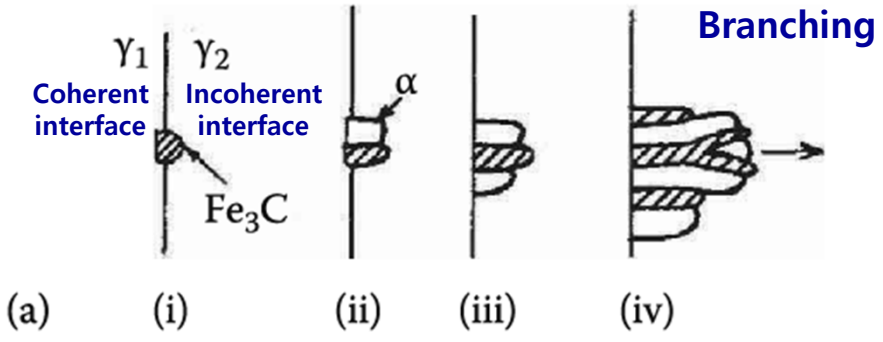

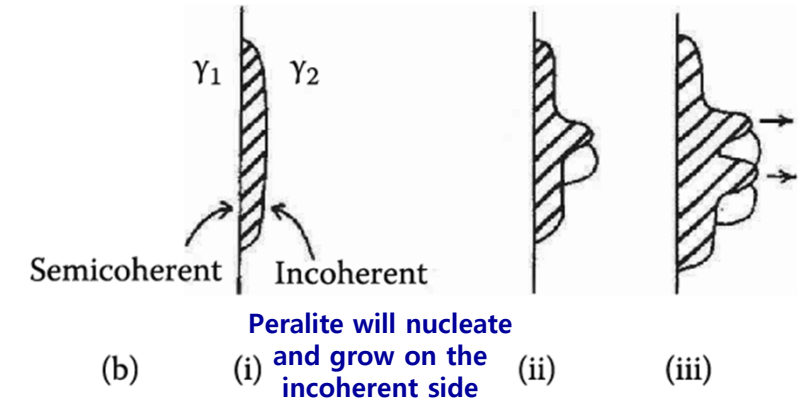

Peralite will nucleate and grow on the incoherent side

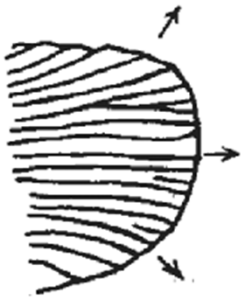

(c) A perlite colony at a later stage of growth

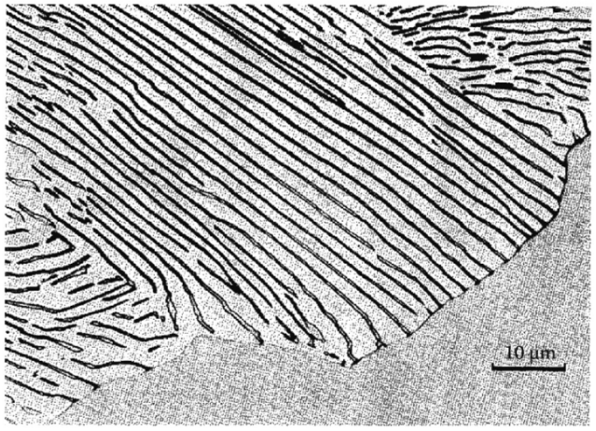

(a) On a "clean" GB.

(i) **Cementite nucleates on GB with coherent interface and orientation relationship with γ_1 and incoherent interface with γ_2.**

(ii) **α nucleates adjacent to cementite also with a coherent interface and orientation relationship with γ_1. (This also produces an orientation relationship between the cementite and the ferrite).**

(iii) **The nucleation process repeats side ways, while incoherent interfaces grow into γ_2.**

(iv) **New plates can also form by a branching mechanism.**

(b) When a proeutectoid phase (cementite or ferrite) already exists on that boundary, pearlite will nucleate and grow on the incoherent side. A different orientation relationship between the cementite and the ferrite results in this case.

(c) Pearlite colony at a latest stage of growth.

Pearlite grows into the austenite grain with which it does not have an orientation relationship.

Growth of Pearlite: analogous to the growth of a lamellar eutectic

Min. possible: $(S^*) \propto 1/\Delta T$ / Growth rate : mainly lattice diffusion $v = kD_c^{\gamma}(\Delta T)^2$

Interlamellar spacing of pearlite colonies mainly boundary diffusion $v = kD_b(\Delta T)^3$

Relative Positions of the Transformation curves for Pearlite and Bainite in Plain Carbon Eutectoid Steels.

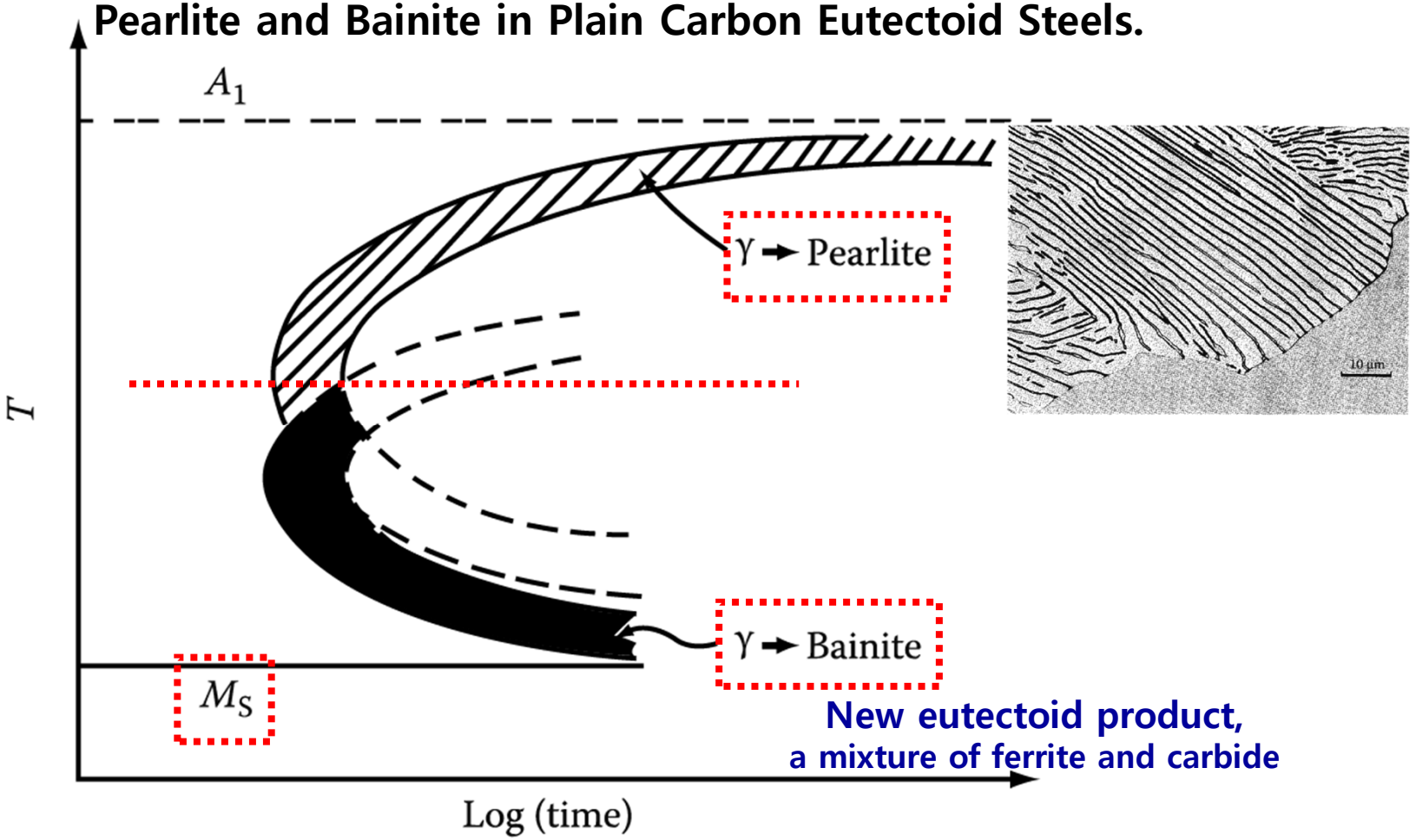

Figure 5.64 Schematic diagram showing relative positions of the transformation curves for pearlite and bainite in plain carbon eutectoid steel.

5.8.2 Bainite Transformation

The microstructure of bainite depends mainly on the temperature at which it forms.

Upper Banite in medium-carbon steel

At high temp. 350 ~ 550°C, ferrite laths, K-S relationship, similar to Widmanstäten plates

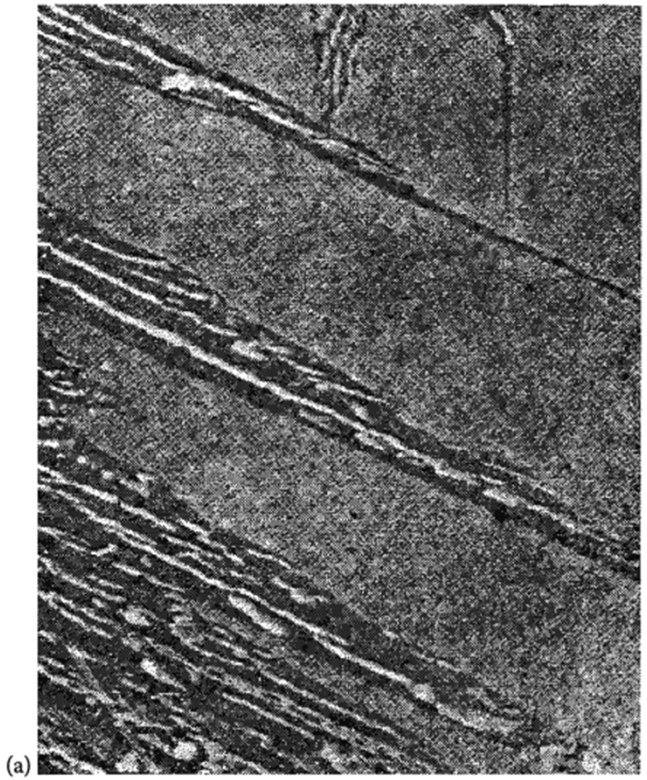

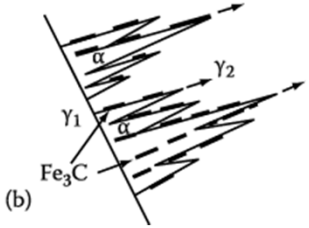

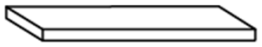

(b) Schematic of growth mechanism. Widmanstatten ferrite laths growth into γ_2. Cementite plates nucleate in carbon-enriched austenite.

Lower Bainite in 0.69wt% C low-alloy steel

At sufficiently low temp. laths → plates

Carbide dispersion becomes much finer, rather like in tempered M.

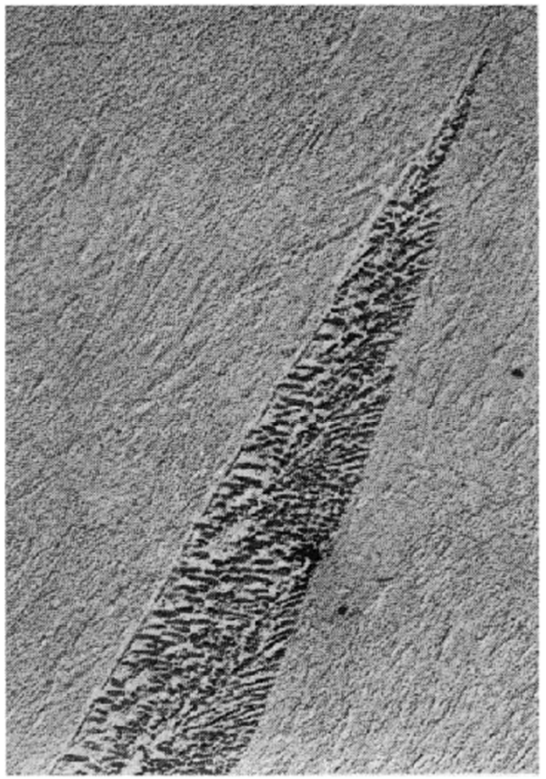

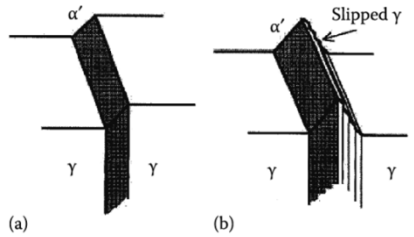

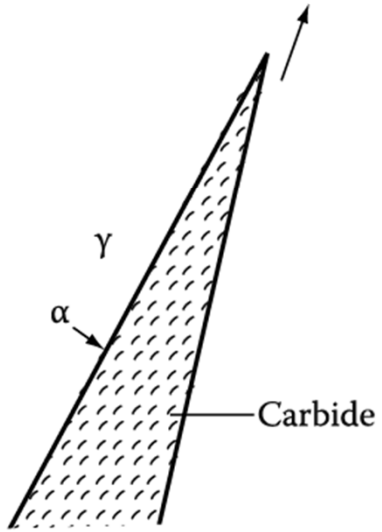

Surface tilts by bainite trans. like M trans.
Due to Shear mechanism/ordered military manner

(b) A possible growth mechanism. α/γ interface advances as fast as carbides precipitate at interface thereby removing the excess carbon in front of the α.

At the highest temp. where pearlite and bainite grow competitively.

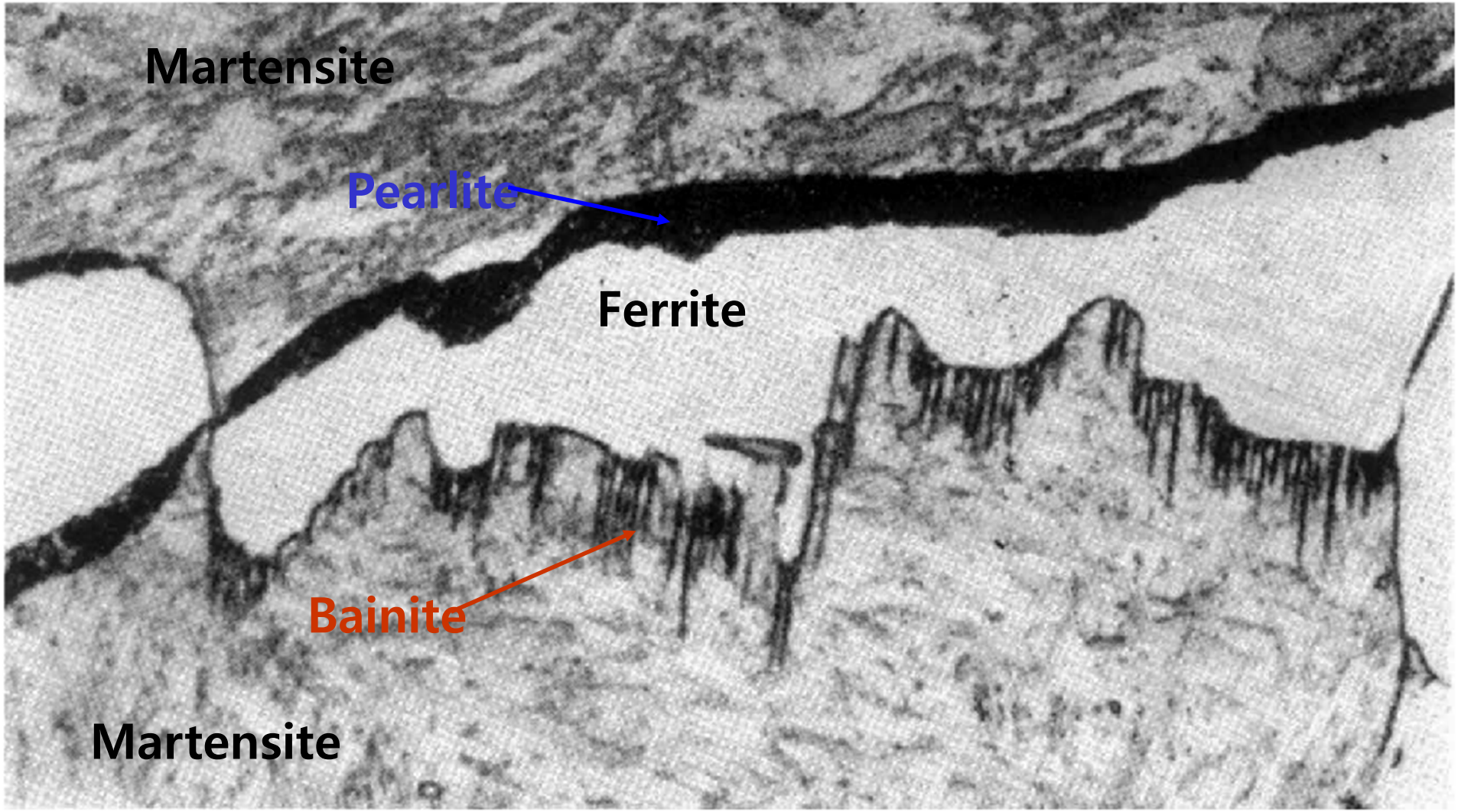

Fig. 5.67 Hypoeutectoid steel (0.6% C) partially transformed for 30 min at 710 ℃. Inefficiently quenched. Bainitic growth into lower grain of austenite and pearlitic growth into upper grain during quench (x1800).

Pearlite : no specific orientation relationship

Bainite : orientation relationship

5.8.3 The effect of alloying elements on hardenability

: adding alloying elements to steels → delay to time required for the decomposition into ferrite and pearlite → M trans under slower cooling rate → increase hardenability

* Main factor limiting hardenability is the rate of formation of pearlite at the nose of the C curve in the TTT diagram.

- Austenite stabilizer (Mn, Cu, Ni) – depress A3 temperature
- Ferrite stabilizer (Cr, Mo, Si) – increase A3 temperature

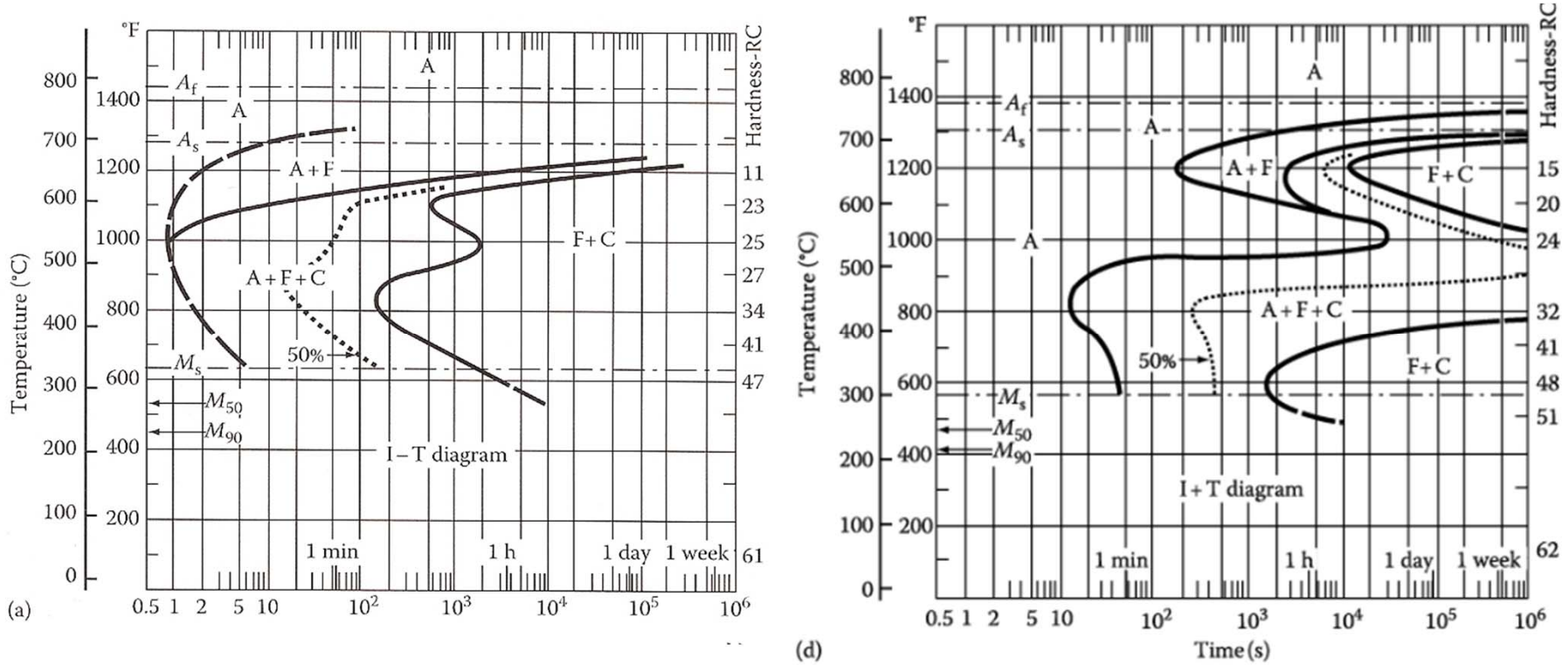

Figure 5.73 TTT diagrams for two commercial low-alloy steels all of which (a) contain roughly 0.4% C and 1% Mn and (b) contains 0.8% Cr, 0.3% Mo, and 1.8% Ni

5.8.4 - 5.8.6 skip

5. Diffusion Transformations in solid

(c) Order-Disorder Transformation

$$\alpha \rightarrow \alpha'$$

Disorder (high temp.) Order (low temp.)

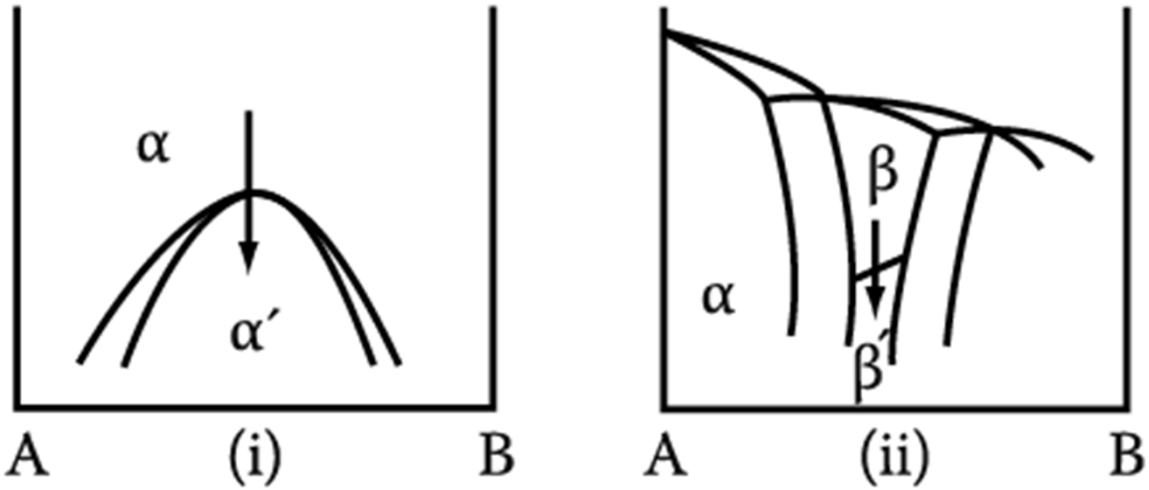

(d) Massive Transformation

: The original phase decomposes into one or more new phases which have the same composition as the parent phase, but different crystal structures.

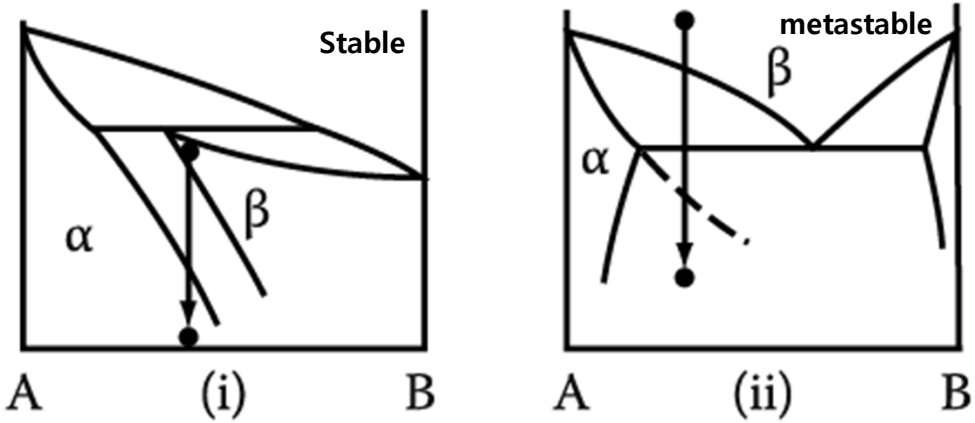

$$\beta \rightarrow \alpha$$

(e) Polymorphic Transformation

In single component systems, different crystal structures are stable over different temperature ranges.

5.9 Massive Transformation

: The original phase decomposes into one or more new phases which have the same composition as the parent phase, but different crystal structures.

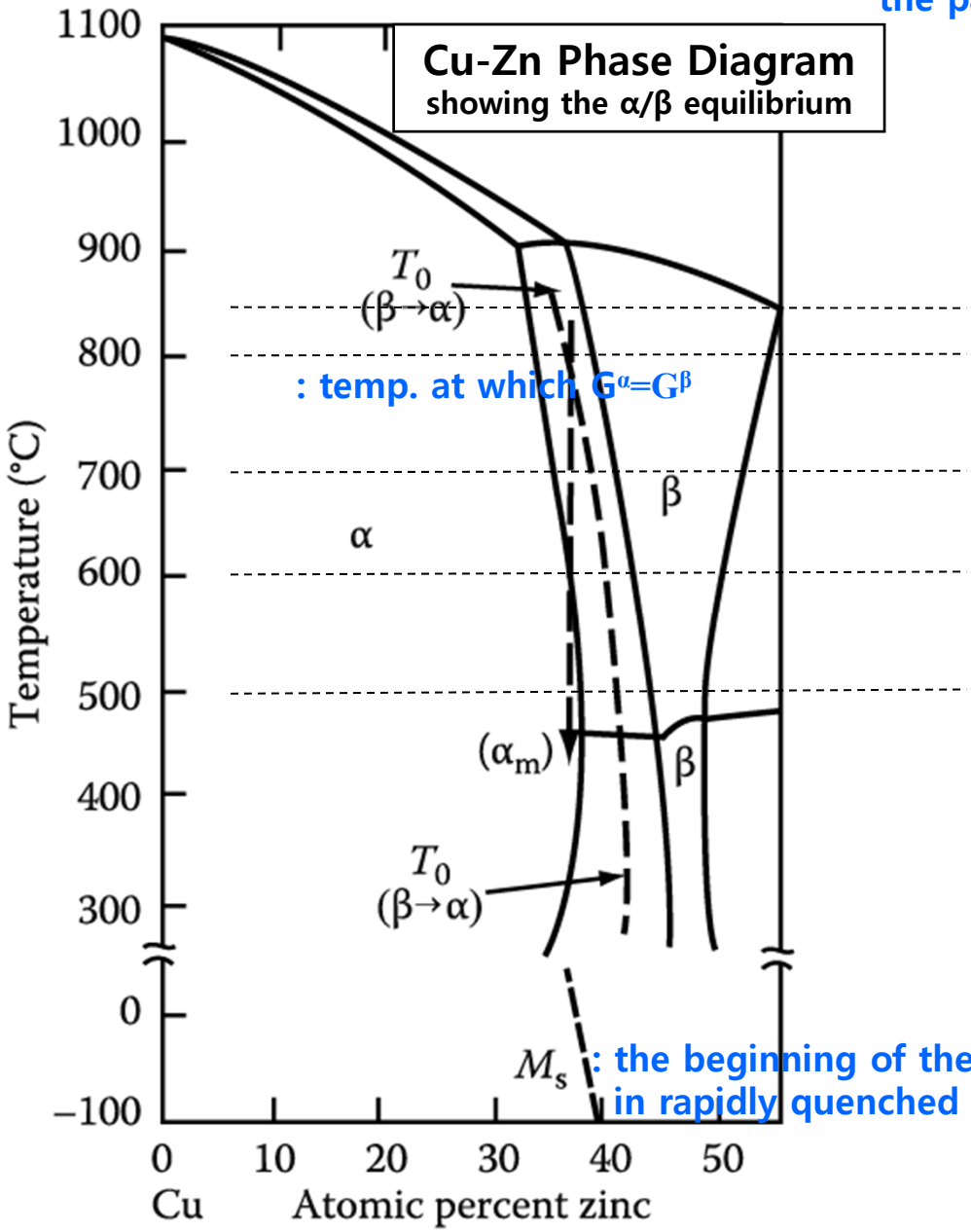

: temp. at which $G^{\alpha}=G^{\beta}$

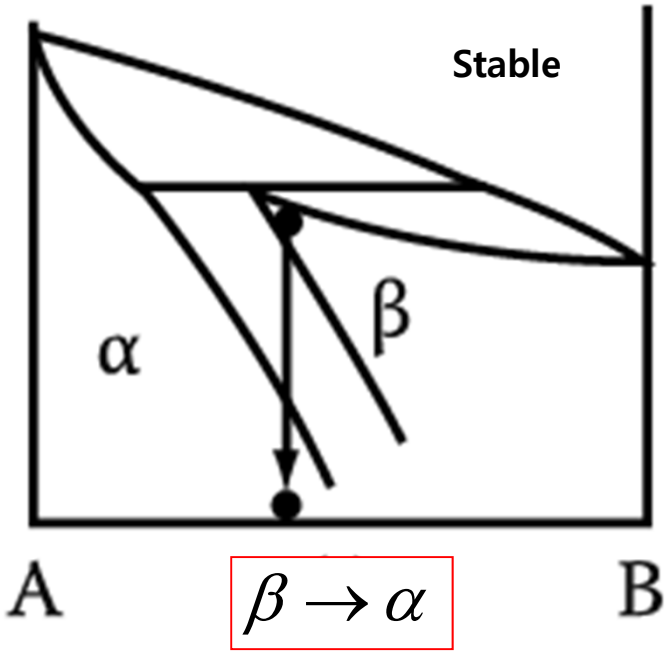

Free energy-composition curves for α and β at 850°C, 800°C, 700°C and 600°C?

M_s : the beginning of the M transformation in rapidly quenched specimens.

5.9 Massive Transformation

Free energy-composition curves for α and β

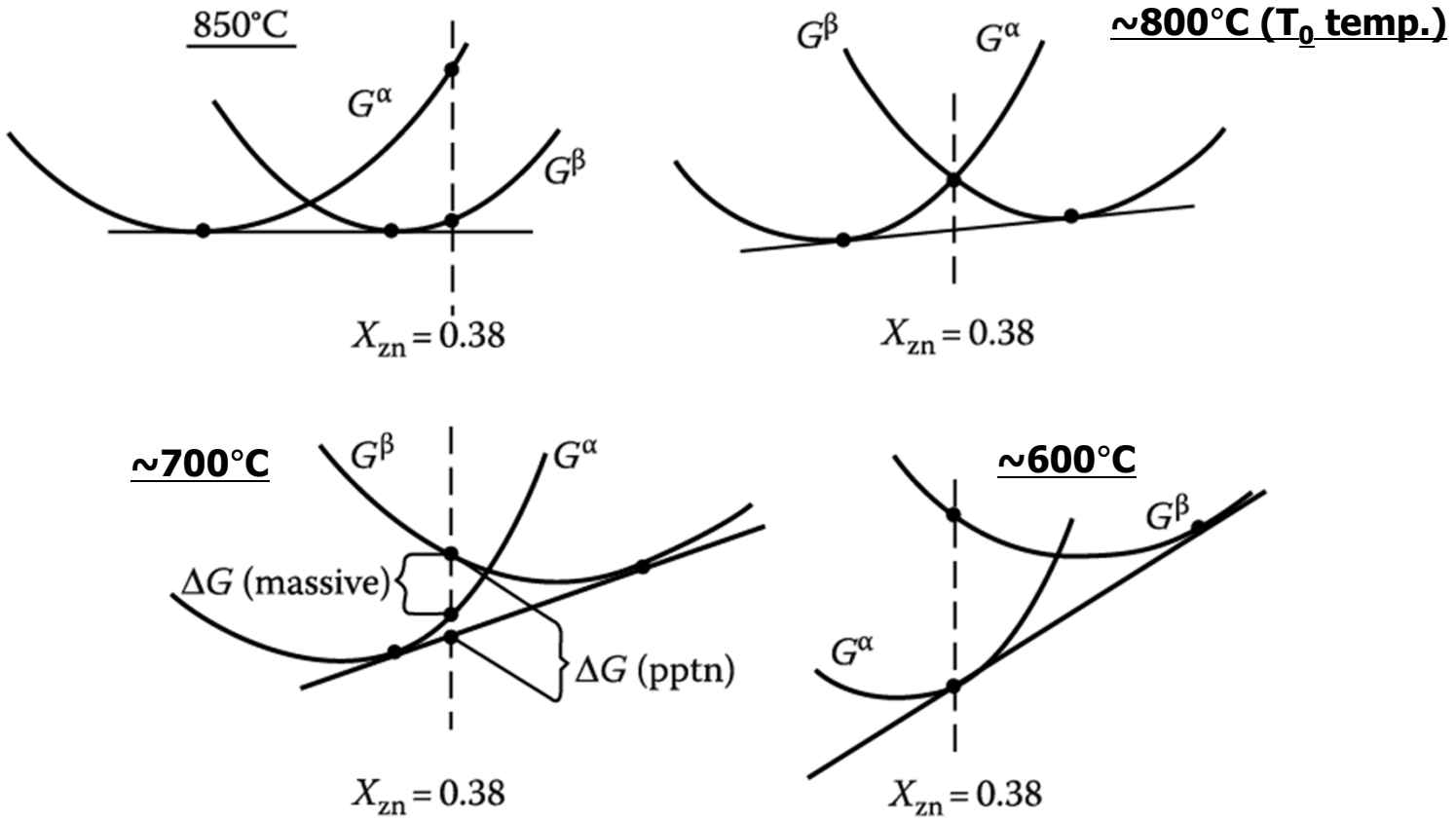

Fig. 5.86 A schematic representation of the free energy-composition curves for α and β in the Cu-Zn system at various temperatures.

At the thermodynamic point of view, it may possible for a massive trans. to occur within the two-phase region of the phase dia. anywhere below the T_0 temp.. But, in practice, there is evidence that massive trans. usually occur only within the single-phase region of the phase diagram

5.9 Massive Transformation

Massive α formed at the GBs of β and grow rapidly into the surrounding β

: a diffusionless civilian transformation (change of crystal structure without a change of composition)

Migration of the α/β interfaces~ very similar to the migration of GBs during recrystallization of single-phase material but, driving force ~ orders of magnitude greater than for recrystallization→ rapid growth: a characteristic irregular appearance.

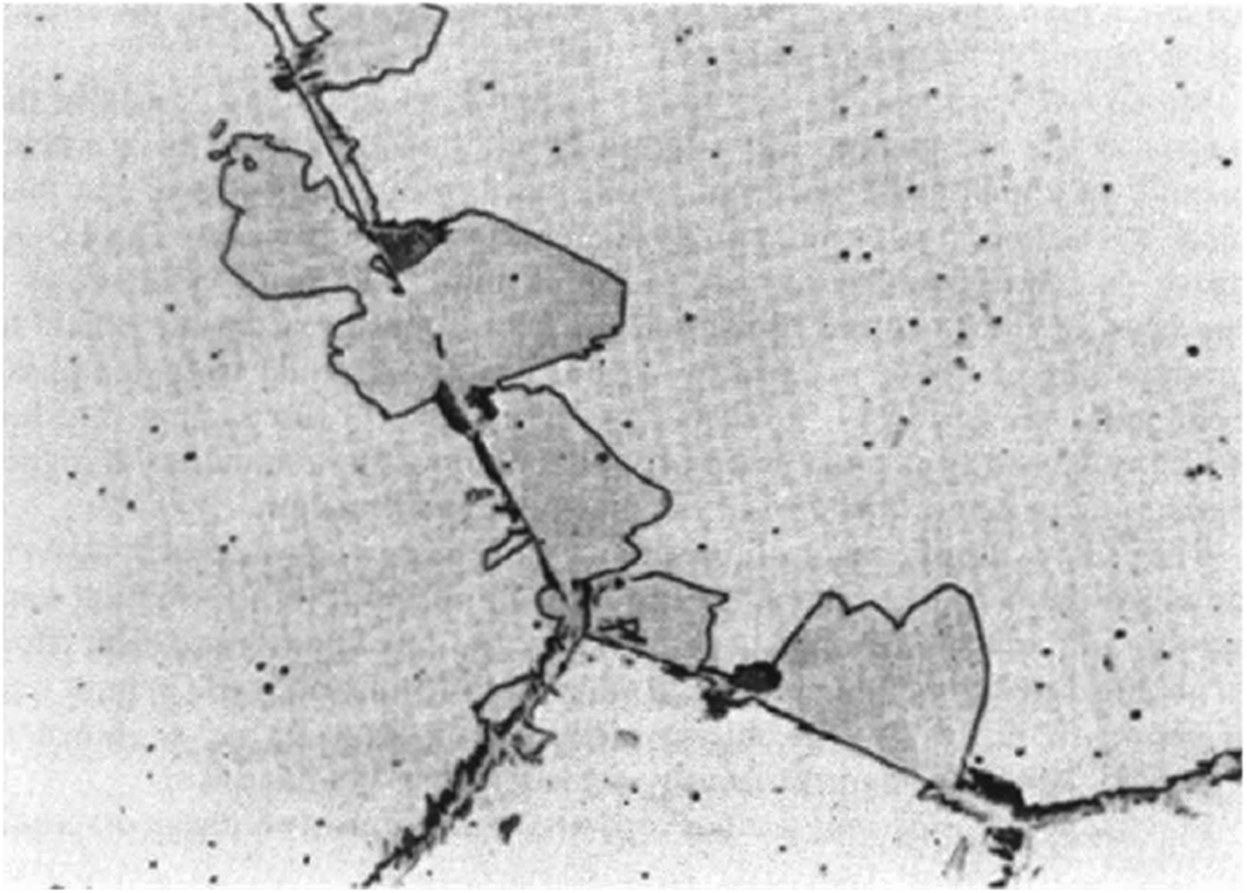

Figure 5.85 Massive a formed at the GBs of β in Cu-38.7wt% Zn quenched from 850℃ in brine at 0℃. Some high temperature precipitation has also occurred on the boundaries.

* Massive, Martensite Transformation

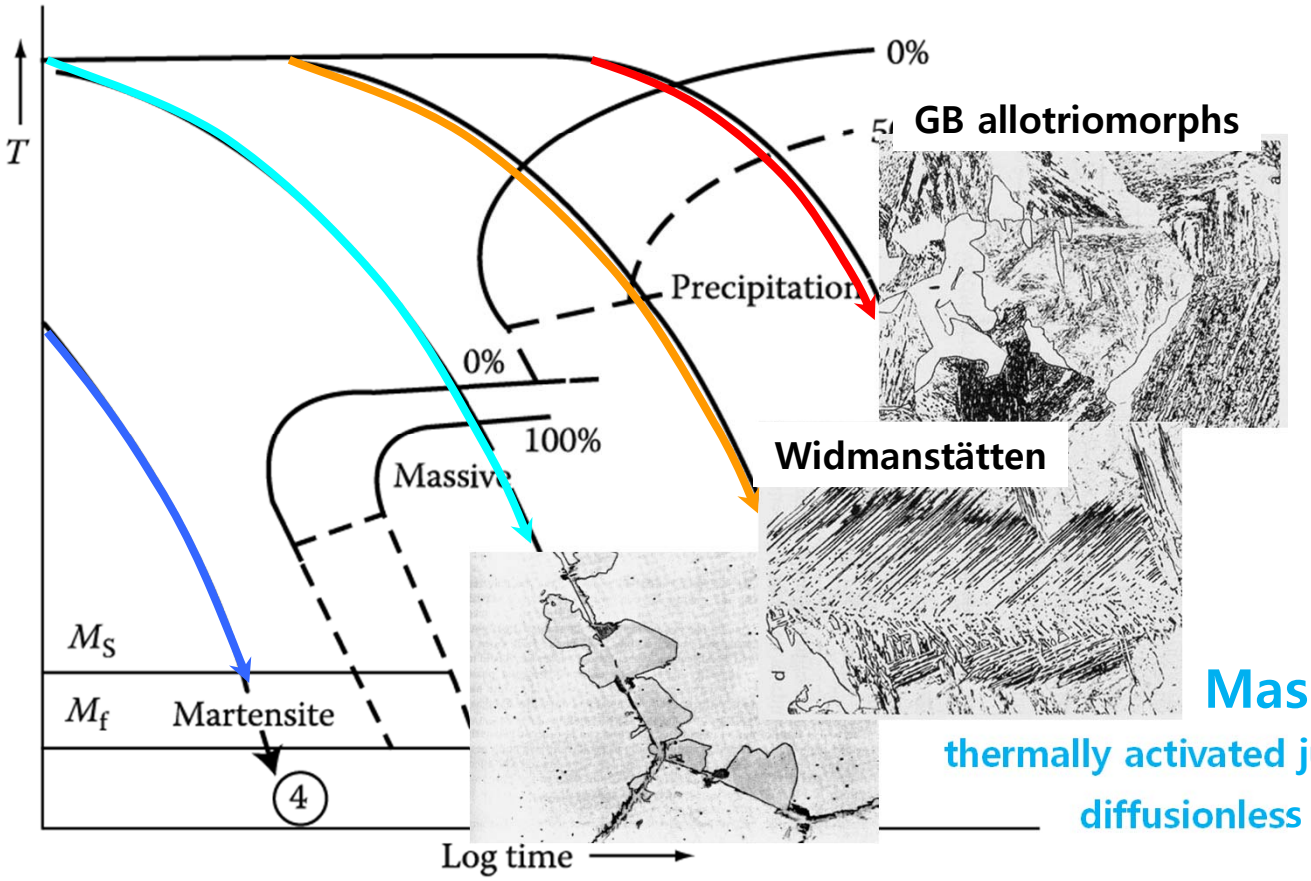

Martensite

Massive Transformation

thermally activated jumping across the α/β interface

diffusionless civilian transformation

β is sheared into α by the cooperative move-ment of atoms across a glissile interface

diffusionless military transformation

Martensite Transformation

Fig. 5.75 A possible CCT diagram for systems showing a massive transformation. Slow cooling (1) produces equiaxed α. Widmanstatten morphologies result from faster cooling (2). Moderately rapid quenching (3) produces the massive transformation, while the highest quench rate (4) leads to a martensitic transformation.

5.9 Massive Transformation : γ→α transformation in iron and its alloy

Effect of Cooling Rate on the Transformation Temperature at which transformation starts in pure iron

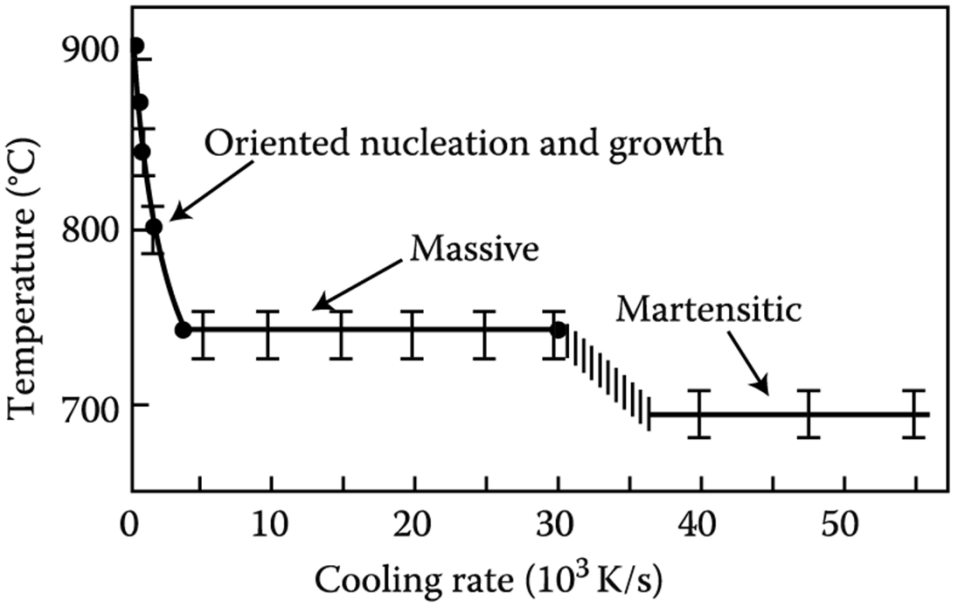

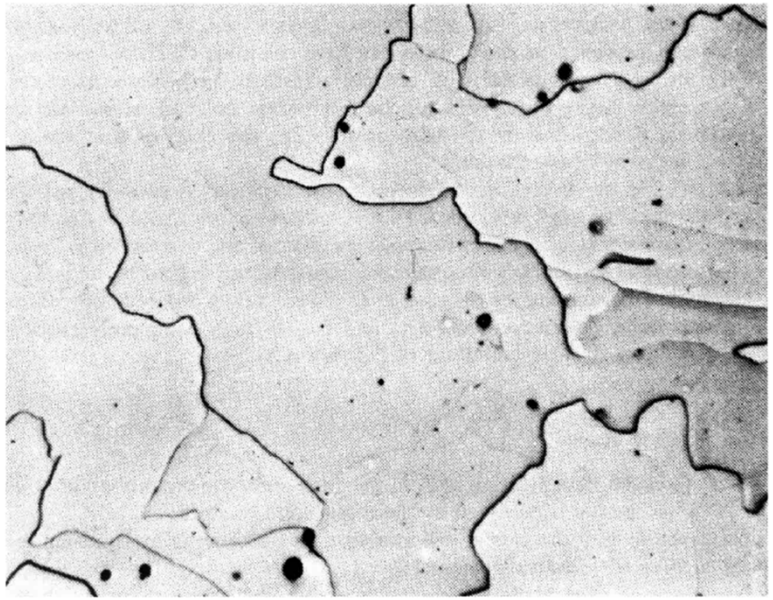

Massive a in an Fe-0.002wt%C
Quenched into iced brine from 1000 °C
: characteristically irregular α/α GBs.

5.9 Massive Transformation

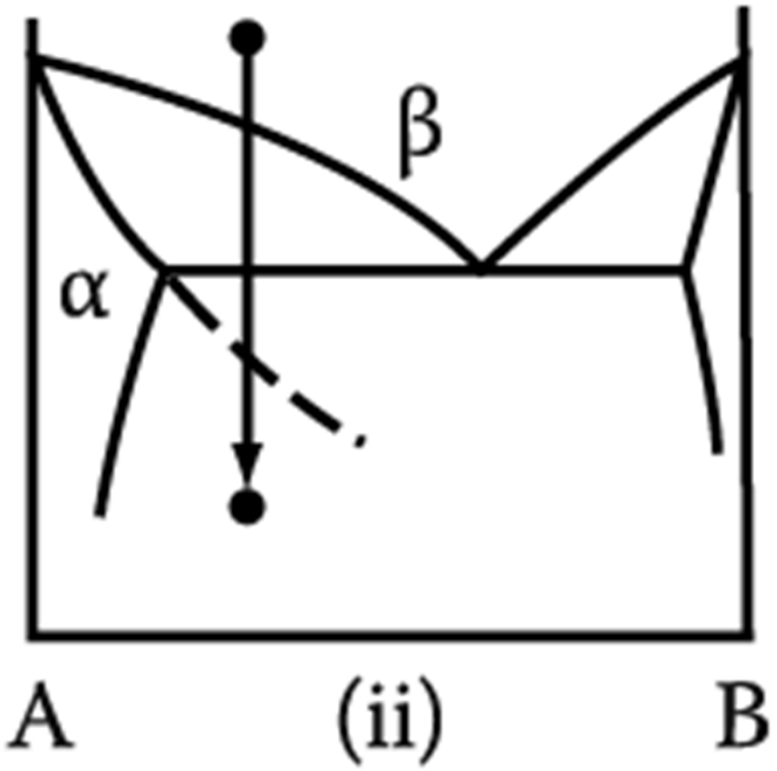

Metastable phases can also form massively.

It is not even necessary for the transformation product to be a single phase: two phases, at least one of which must be metastable, can form simultaneously provided they have the same composition as the parent phase.

5.10 & 5.11 skip

5. Diffusion Transformations in solid

: diffusional nucleation & growth

(a) Precipitation

$$\alpha' \rightarrow \alpha + \beta$$

Metastable supersaturated
Solid solution

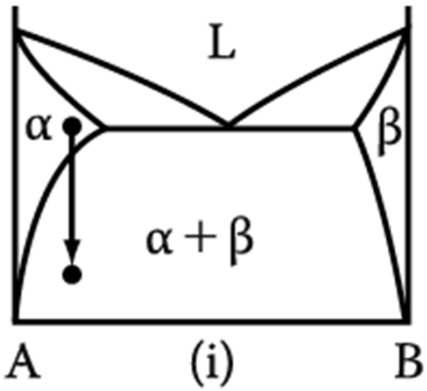

Homogeneous Nucleation

$$\Delta G = -V\Delta G_V + A\gamma + V\Delta G_S$$

Heterogeneous Nucleation

$$\Delta G_{het} = -V(\Delta G_V - \Delta G_S) + A\gamma - \Delta G_d$$

$$N_{\text{hom}} = \omega C_0 \exp\left(-\frac{\Delta G_m}{kT}\right)\exp\left(-\frac{\Delta G^*}{kT}\right)$$

➡ suitable nucleation sites ~ nonequilibrium defects
(creation of nucleus~destruction of a defect($-\Delta G_d$))

(b) Eutectoid Transformation

Composition of product phases differs from that of a parent phase.
→ long-range diffusion

Which transformation proceeds by short-range diffusion?

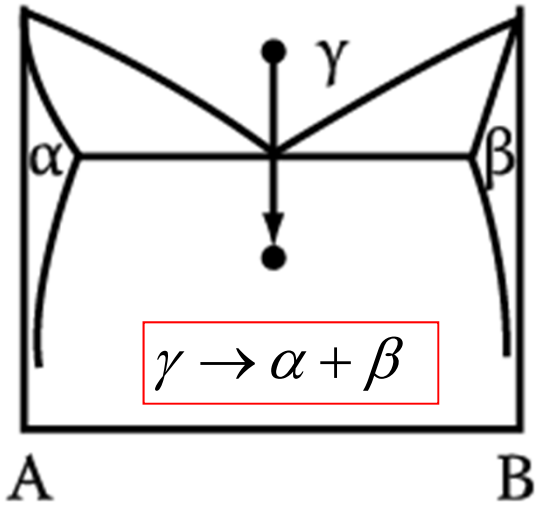

5. Diffusion Transformations in solid

(c) Order-Disorder Transformation

$$\alpha \rightarrow \alpha'$$

Disorder (high temp.) Order (low temp.)

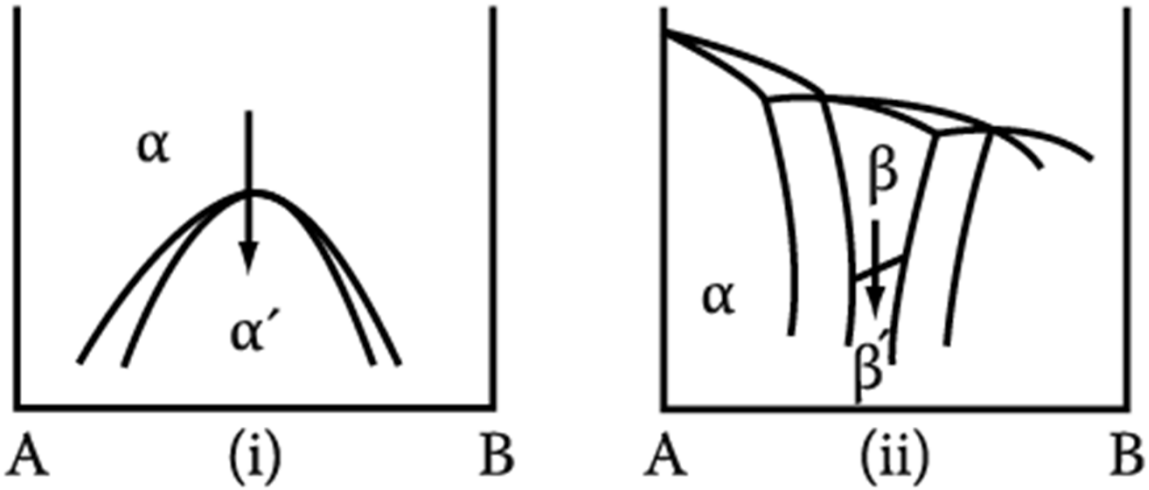

(d) Massive Transformation

: The original phase decomposes into one or more new phases which have the same composition as the parent phase, but different crystal structures.

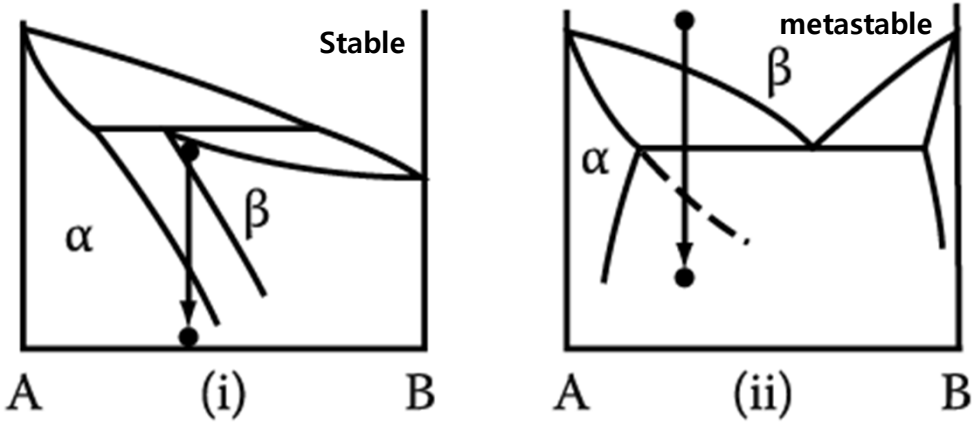

$$\beta \rightarrow \alpha$$

(e) Polymorphic Transformation

In single component systems, different crystal structures are stable over different temperature ranges.

*** Homework 5 : Exercises 5 (pages 379-381)**

until 19th December (before exam)

Good Luck!!